FINAL BACHELOR'S PROJECT

Material engineering degree

MICROSTRUCTURAL DESIGN OF A NEW ZIRCONA BASED MATERIAL FOR DENTAL IMPLANTS

Project Report and Annexes

Author: Raúl Agut López
Director/a: Joan Josep Roa Rovira
Co-Director/a: Montserrat Español Pons
Announcement: June 2021

Resum

Un dels materials més rellevants en les últimes dècades és la zircònia (ZrO_2) degut a les seves excel·lents propietats mecàniques. Degut a les seves propietats, aquest material s'ha utilitzat àmpliament en aplicacions dentals i ortopèdiques. Avui en dia continua sent un material àmpliament estudiat, ja que es volen trobar noves maneres per millora l'osteointegració i prevenir els problemes relacionats amb la degradació hidrotèrmica.

En aquest projecte final de grau (TFG), l'objectiu principal és aconseguir conformar un implant dental. S'ha intentat conformar amb tres materials base zircònia; $3Y-ZrO_2$, $12Ce-ZrO_2$ i un composite de $3Y/12Ce-ZrO_2$. Per tal d'aconseguir aquest objectiu s'han utilitzat dues tècniques, la impressió 3D, mitjançant la tècnica del Robocasting també coneguda com Direct Ink Writing (DIW), i el fresat.

En el transcurs del TFG, s'ha hagut de caracteritzar la pols de partida, en termes de mida de gra i cristal·linitat, així com les propietats tant microestructurals com mecàniques mitjançant tècniques avançades de caracterització (com per exemple microscòpia electrònica de rastreig, difracció de rajos X, entre altres) dels diferents materials tant processats mitjançant tècniques de processat tradicional, Cold Isostatic Pressing (CIP) com mitjançant impressió 3D. Finalment, s'han investigat les propietats tant microestructurals com mecàniques en condicions de servei, per això les mostres han estat degradades hidrotèrmicament.

La caracterització de la pols així com la seva cristal·linitat ha permès observar que els diferents materials d'estudi en aquest TFG poden ser impresos en 3D, i que les seves propietats mecàniques resultants no es veuen molt afectades en comparació amb les propietats obtingudes quan els materials han estat conformats mitjançant tècniques tradicionals. A més s'ha pogut comprovar com el material composite $85/15-ZrO_2$ no ha patit degradació hidrotèrmica en concordança amb el que hi ha reportat a la literatura.

Pel que fa a la impressió d'implants, s'ha aconseguit imprimir l'implant amb diferents longituds, 24, 17 i 12 mm el qual implica un 600%, 400 % y 200% superior a l'original, respectivament; fet que posa de manifest que la tècnica emprada d'impressió 3D es una tècnica viable per a realitzar aquest tipus de geometria i, amb un control més precís de la pols de partida així com dels paràmetres d'impressió, es pot arribar a imprimir amb les mesures reals. Per contra, les tècniques de mecanitzat tradicionals no han donat els resultats esperats, ja que les eines usades s'han vist superades per l'alta duresa dels materials estudiats en aquest TFG.

Resumen

Uno de los materiales más relevantes en las últimas décadas es la circonia (ZrO_2) debido a sus excelentes propiedades mecánicas. Debido a sus propiedades, este material se ha utilizado ampliamente en aplicaciones dentales y ortopédicas. Hoy en día continúa siendo un material ampliamente estudiado, puesto que se quiere encontrar nuevas maneras para mejorar la osteointegración y prevenir problemas relacionados con la degradación hidrotérmica.

En este proyecto final de grado (TFG), el objetivo principal es conseguir conformar un implante dental. Se ha intentado conformar con tres materiales base circonia; $3Y-ZrO_2$, $12Ce-ZrO_2$ y un composite $3Y/12Ce-ZrO_2$. Para conseguir este objetivo se han utilizado dos técnicas, la impresión 3D, mediante la técnica del Robocasting también conocida como Direct Ink Writing (DIW), y el fresado.

En el transcurso del TFG, se ha tenido que caracterizar el polvo de partida, en términos de tamaño de grano y cristalinidad, así como las propiedades tanto microestructurales como mecánicas mediante técnicas avanzadas de caracterización (como por ejemplo microscopia electrónica de barrido, difracción de rayos X, entre otros) de los diferentes materiales tanto procesados mediante técnicas de procesado tradicional, Cold Isostatic Pressing (CIP) como mediante impresión 3D. Finalmente, se han investigado las propiedades tanto microestructurales como mecánicas en condiciones de servicio, por eso las muestras han sido degradadas hidrotermalmente.

La caracterización del polvo así como su cristalinidad ha permitido observar que los diferentes materiales estudiados en este TFG pueden ser imprimidos en 3D, y que sus propiedades mecánicas resultantes no se ven muy afectadas en comparación con las propiedades obtenidas cuando los materiales han sido conformados mediante técnicas tradicionales. Además, se ha podido comprobar como el material composite $85/15-ZrO_2$ no ha sufrido degradación hidrotérmica en concordancia con lo que hay reportado en la literatura.

En cuanto a la impresión de implantes, se ha conseguido imprimir el implante con diferentes longitudes, 24, 17 y 12 mm lo cual implica un 600%, 400% y 200% de escalado respecto al tamaño original, respectivamente; hecho que pone de manifiesto que la técnica empleada de impresión 3D es una técnica viable para realizar este tipo de geometría y, con un control más preciso del polvo de partida así como de los parámetros de impresión, se puede llegar a imprimir con las medidas reales. Por el contrario, las técnicas de mecanizado tradicionales no han dado los resultados esperados, puesto que las herramientas usadas se han visto superadas por la alta dureza de los materiales estudiados en este TFG.

UNIVERSITAT POLITÈCNICA DE CATALUNYA
BARCELONA**TECH**
Escola d'Enginyeria de Barcelona Est

Abstract

One of the most important materials in the last decades is the zirconia (ZrO_2) due to its excellent mechanical properties. Due to its properties, this material has been widely used in dental and orthopaedic applications. Nowadays it remains under investigation, as new ways are to be found to improve the osseointegration and prevent the issues related to the hydrothermal degradation.

In this Bachelor's degree project, the main objective is to achieve the shaping of a dental implant. Three zirconia-based materials have been used; $3Y$-ZrO_2, $12Ce$-ZrO_2 and a composite of $3Y/12Ce$-ZrO_2. To achieve this objective, two techniques have been used, 3D printing, using the Robocasting technique also known as Direct Ink Writing (DIW), and milling.

In the course of this Bachelor's degree project, it has been necessary to characterise the starting powders, in terms of grain size and crystallinity, as well as the microstructural and mechanical properties by means of advanced characterization techniques (such as scanning electron microscopy, X-Ray Diffraction, among others) of the different materials both processed by traditional processing techniques, Cold Isostatic Pressing (CIP) and 3D printing. Finally, both microstructural and mechanical properties have been investigated under service conditions, so the samples have been hydrothermally degraded.

The characterization of the powder as well as its crystallinity has allowed to observe that the different materials studied in this Bachelor's degree project can be 3D printed, and that their resulting mechanical properties are not much affected in comparison with the properties obtained when the materials have been made by traditional techniques. Furthermore, it has been verified that the $85/15$-ZrO_2 composite materials has not suffered hydrothermal degradation as accordance in the literature.

As for the 3D printing of implants, it has been possible to print the implant with different lengths, 24, 17 and 12 mm, which implies 600%, 400% and 200% more than the original, respectively; this fact shows that the 3D printing technique used is a viable technique for this type of geometry and, with more precise control of the starting powder as well as the 3D printing parameters, it is possible to print with the real measurements. On the other hand, traditional machining techniques have not given the expected results, since the tools used have been overcome by the high hardness of the materials studied in this bachelor's degree project.

Acknowledgments

I would like to thank Joan Josep Roa for the opportunity to do this project and for guiding me through its development

On the other hand, I would like to thank my family for the encouragement they given me during the whole process.

UNIVERSITAT POLITÈCNICA DE CATALUNYA
BARCELONATECH
Escola d'Enginyeria de Barcelona Est

Figure list

UNIVERSITAT POLITÈCNICA DE CATALUNYA
BARCELONATECH
Escola d'Enginyeria de Barcelona Est

UNIVERSITAT POLITÈCNICA DE CATALUNYA
BARCELONA**TECH**
UPC   Escola d'Enginyeria de Barcelona Est

Table list

UNIVERSITAT POLITÈCNICA DE CATALUNYA
BARCELONATECH
Escola d'Enginyeria de Barcelona Est

Glossary

ZrO$_2$: Zirconium oxide

3Y-ZrO$_2$: 3 mol. % of Y$_2$O$_3$-ZrO$_2$

12Ce-ZrO$_2$: 12 mol. % of CeO$_2$-ZrO$_2$

12Ce/3Y-ZrO$_2$: Composite with 85% 12Ce-ZrO$_2$ and 15% 3Y-ZrO$_2$

***m*-**: monoclinic phase

***t*-**: tetragonal phase

***c*-**: cubic phase

Y$_2$O$_3$: Yttrium Oxide

CaO: Calcium Oxide

MgO: Magnesium Oxide

CeO$_2$: Cerium Oxide

CaF$_2$: Calcium Fluoride

TZP: Tetragonal Zirconia Polycrystal

PSZ: Partially Stabilized Zirconia

FSZ: Fully Stabilized Zirconia

LTD: Low Temperature Degradation

Al$_2$O$_3$: Aluminium Oxide

NTM: Non-Traditional Machining

RUM: Rotatory **U**ltrasonic Machining

LM: Laser Machining

DIW: Direct Ink Writing

UNIVERSITAT POLITÈCNICA DE CATALUNYA
BARCELONA**TECH**
UPC Escola d'Enginyeria de Barcelona Est

CIP: Cold Isostatic Pressing

LD: Laser Diffraction

OM: Optical Microscopy

SEM: Scanning Electron Microscopy

FE-SEM: Field Emission Scanning Electron Microscopy

XRD: X-Ray Diffraction

HV: Vickers Hardness

UNIVERSITAT POLITÈCNICA DE CATALUNYA
BARCELONATECH
Escola d'Enginyeria de Barcelona Est

Index

UNIVERSITAT POLITÈCNICA DE CATALUNYA
BARCELONATECH
Escola d'Enginyeria de Barcelona Est

UNIVERSITAT POLITÈCNICA DE CATALUNYA
BARCELONA**TECH**
Escola d'Enginyeria de Barcelona Est

0. Preface

0.1. Motivation

Nowadays we are living an increasingly hasty evolution of society caused by the rapid evolution of technology, these changes bring new needs that companies and researchers have to solve, finding new alternatives and new processes to improves people's lives. Years ago, thanks to engineering, society underwent great changes. With the development of communication systems and computer capable of high-speed complex calculations, we have been able to create complex systems, like advanced microscopy or the emergence of the aerospace industry.

As a degree student, this Bachelor's project seems like the perfect way to close a stage and to be able to apply what has been learnt and be able to acquire more knowledge by learning how to use advanced characterization techniques, like scanning electron microscopy, nanoindentation, among others. This degree has made me acknowledge the importance of materials engineering. The study of biomaterials, especially ceramic materials, had been one of my favourite subjects. With this project I want to learn how research in this field is carried out in order to prepare myself for the master's degree the next year and start it motivated.

During my degree several times zirconia has been mentioned as a very interesting material because of its mechanical and chemical properties, as well as their applicability as a biomaterial. The main motivation is to be able to study and work with this promising material, as well as to learn various conforming ceramic techniques, from a tradition to more advance techniques, like machining and such as 3D printing of ceramics, respectively.

UNIVERSITAT POLITÈCNICA DE CATALUNYA
BARCELONA**TECH**
Escola d'Enginyeria de Barcelona Est

0.2. Previous Requirements

For the correct development of this bachelor's degree project, the following regulations have been read before starting it and have been consulted during its development:

(1) Vickers hardness test: UNE-EN ISO 6507-2018
- Part 1: Test method (ISO 6507-1:2018).
- Part 2: Verification and calibration of testing machines (ISO 6507-2:2018).
- Part 3: Calibration of reference blocks (ISO 6507-3:2018).

(2) Standard Test Methods for Determining Average Grain Size: ASTM E112

UNIVERSITAT POLITÈCNICA DE CATALUNYA
BARCELONATECH
Escola d'Enginyeria de Barcelona Est

1. Introduction

1.1. Zirconia based ceramic

1.1.1. General information

Zirconia (ZrO_2) is one of the most important ceramic oxides due to its excellent mechanical properties. But until the 1975 it was used only for refractory applications, due to the martensitic phase transformation from tetragonal to monoclinic phase [1, 2]. Nowadays, this material is used in new high technology applications, like wear applications, thermal barrier coatings, biomedical applications among others. This is possible thanks to the investigation of the phase transformation and the knowledge of the stabilisers that improve the processing of the material. These two concepts will be explained later in the corresponding section.

1.1.2. Microstructure

ZrO_2 is a polymorphic material, which presents three different crystallographic phases depending on its composition and temperature (3) as it is shown in **Figure 1**: monoclinic (*m-),* tetragonal (*t-*) and cubic (*c-*).
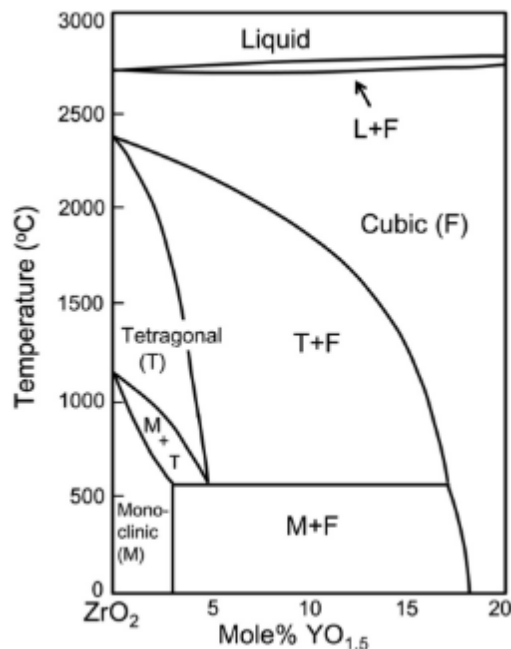
Figure 1. *Phase diagram of yttria (Y_2O_3)-stabilized ZrO_2 (4).*

The *m*-phase (**Figure 2a**) is stable at room temperature and it will do not change until 1170ºC. The *t*-phase (**Figure 2b)** is formed between temperatures ranging from 1170ºC to 2370ºC. Above 2370ºC the *c*-phase (**Figure 2c)** is stable (5). The transition between the *m*- and the *t*-phase involves a large volume expansion.
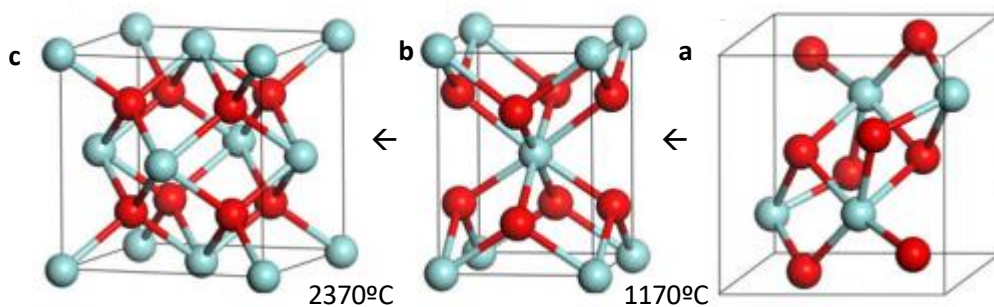
Figure 2. *Representation of the crystallographic phases of Zirconia with the temperature of the three polymorphs. (cubic, tetragonal and monoclinic) (6).*

1.1.3. Stabilization of Zirconia

In 1975, Garvie presented a relation between Zirconia and Steel, mainly because the mechanical properties of Zirconia and also other analogies between this two systems (2). He showed that 3Y-ZrO$_2$ exhibits a transformation toughening mechanism that stops crack propagation. This discovery and the good properties of 3Y-ZrO$_2$ as a material choice for a wide variety of high-performance applications like biomedical or wear applications.

The *t*- and *c*-ZrO$_2$ phases were known as stable only at high temperatures. But it was discovered that they could be stabilized at room temperature adding some specific doping elements.

In this sense, to obtain the *t*- and *c*-phases is necessary stabilize the pure ZrO$_2$ with other oxides, allowing the stabilization of the *t*-ZrO$_2$ phase at room temperature and avoiding the phase transformation during the cooling process.

On the other hand, the *m*-ZrO$_2$ phase presents a lower symmetry and a complex geometric structure. It is stable at room temperature because each Zr cation is in sevenfold coordination to oxygen anions, and there are two non-equivalent oxygen sites. When the temperature increase, to accommodate the oxygen vacancies generated, that structure change into a structure where the Zr cations are surrounded by eight oxygen anions. Zr^{4+} ions have eightfold coordination, as *t*- and *c*- phases. The *c*-phase has an ideal fluorite structure (see **Figure 3**) while the t-ZrO$_2$ presents a slightly distorted cubic structure (6).
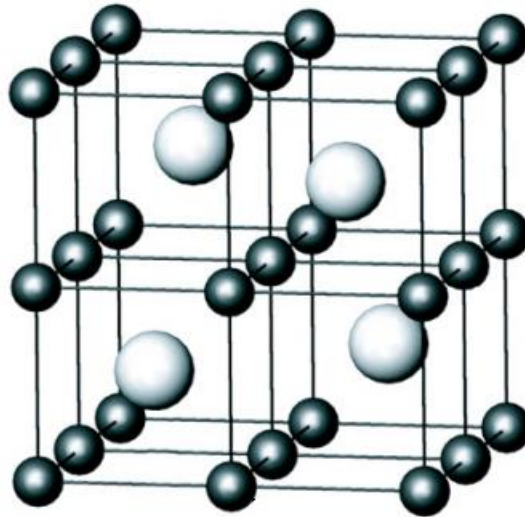
Figure 3. *Unit cell of Fluorite (CaF$_2$) eightfold structure (7).*

Dopants can be classified into trivalent or tetravalent species (according to their oxidation state), and each of these categories, in undersized or oversized, depending on the cation's dimensions compared to Zr. Both parameters strongly affect the stabilization mechanism (8).

By adding trivalent dopants, there is a formation of oxygen vacancies generated for charge compensation. **Figure 5** represents the different models of stabilization process for trivalent dopants. In the case of oversized trivalent dopants (e.g. Y^{+3} or Gd^{+3}) the oxygen vacancies are associated as nearest neighbours to Zr cations, that creates an eight-fold oxygen coordination to the dopant cations. On the other side, when the trivalent dopants are undersized (e.g. Fe^{+3} or Ga^{+3}) they compete with Zr cations for the oxygen vacancies, resulting into a six-fold coordination centres and large disturbance to the nearest neighbours, as shown in **Figure 4** (9).
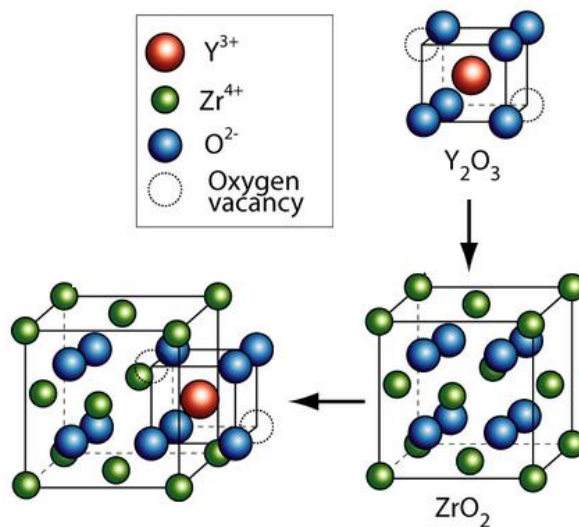
Figure 4. *Formation of oxygen vacancies in the ZrO$_2$ structure with the addition of Y$_2$O$_3$ (10).*

Through the oxygen vacancies associated with Zr cations can provide stability for both *t*- and *c*-ZrO_2, the effectiveness is affected by the availability of oxygen vacancies to Zr cations. Oversized trivalent dopants are more efficient than undersized trivalent dopants [11, 12].
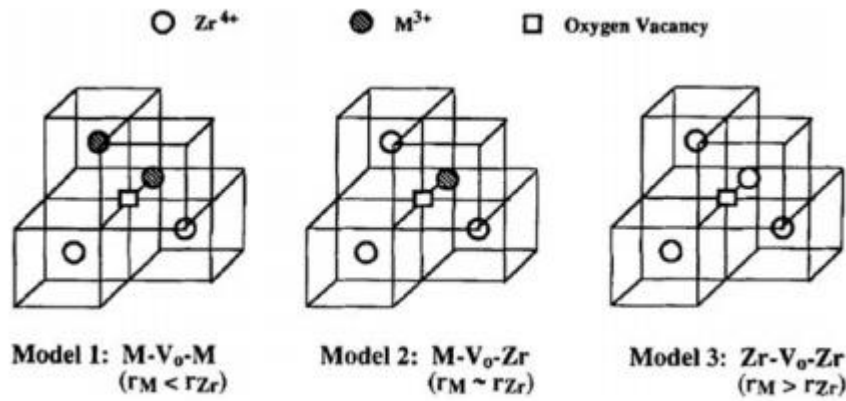
Figure 5. *Illustration of three models for cation-oxygen vacancy association (9).*

As another solutions tetravalent dopants can be used. For oversized dopants, like Ce^{4+}, the structure is deformed and adopts a more symmetric eight-fold coordination, since of their larger size that reduces the tetragonally increasing the stability of the *t*-phase, shown in **Figure 6**. For undersized dopants, like Ge^{+4} the structure is not deformed due to his dimensions and the tetragonally is increased due to the stronger cation oxygen bond (11).
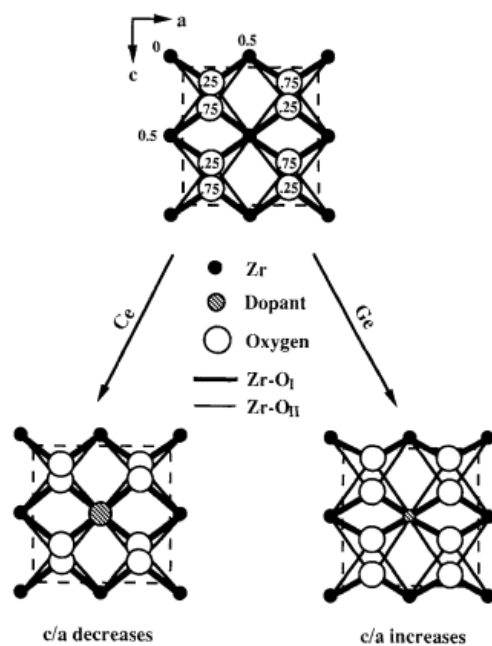
Figure 6. *Schematic illustration of variation of tetragonally of zirconia (11).*

As demonstrated in Ref. (11), the dopant effect on tetragonality decreases according to the type of dopant used, the following list order the dopants from least to the most decrease: trivalent oversized > trivalent undersized > tetravalent oversized > tetravalent undersized.

Nowadays the usually used dopants for stabilizing ZrO_2 are Y_2O_3, CaO, MgO and cerium (CeO_2). The most used dopant to stabilise both *t*-l and *c*-phase at room temperature is Y_2O_3, usually with a 3 and 8 mol. % content, respectively, depending on the final application. $3Y-ZrO_2$ is used for medical applications, while $8Y-ZrO_2$ is used for energy applications.

As said before, the *t*-phase is not thermodynamically stable, because of that is important to show a metastable diagram showing the phase transformation temperature as shown in **Figure 7**.

The shaded area in **Figure 7** indicates the region of metastable t-phase. The metastability of the *t*-phase is proportional of the undercooling below the $t \rightarrow m$ transformation temperature, T_p. If T_p is too low the *t*-phase will be stable, and the transformation phase toughening will not happen. Otherwise, if it is too high the phase transformation will happen spontaneously to *m*- phase upon cooling (12).
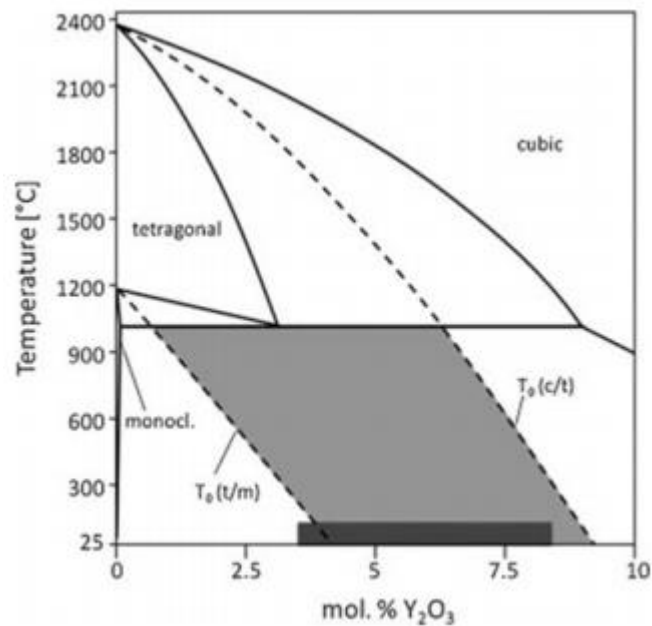
Figure 7. *Y_2O_3-ZrO_2 phase diagram (12).*

1.1.4.   Classification

Currently, there are three generations of ZrO_2 polycrystal materials and it can be classified as: *fully stabilized zirconia (FSZ), partial stabilized zirconia (PSZ), and tetragonal zirconia polycrystals (TZP)* (5).

- **Tetragonal zirconia - TZP**

This kind is considered as a fully tetragonal. The addition of 2-3 mol.% of yttria (Y_2O_3) as a stabilizing agent, allows the sintering of fully t-ZrO_2 grains (13). However it is demonstrated that the 3Y-TZP (or 3Y-ZrO_2) contains some amount of c-ZrO_2, caused by a uneven distribution of the Y^{3+} stabilizer ions (14).

Y_2O_3-stabilized ZrO_2 polycrystals is an important structural ceramic due to its excellent mechanical properties such as hardness, strength and high fracture toughness through the $t \rightarrow m$ phase transformation.

The mechanical properties of 3Y-ZrO_2 strongly depend on its grain size. Above a critical grain size is less stable and has a more spontaneous $t \rightarrow m$ phase transformation, whereas smaller grain size (<1μm) is associated with a lower transformation rate. But, below a determine grain size the transformation is not possible. That's why the sintering conditions have a strong impact on stability and mechanical properties (14). The microstructure of this material is shown in **Figure 8.**
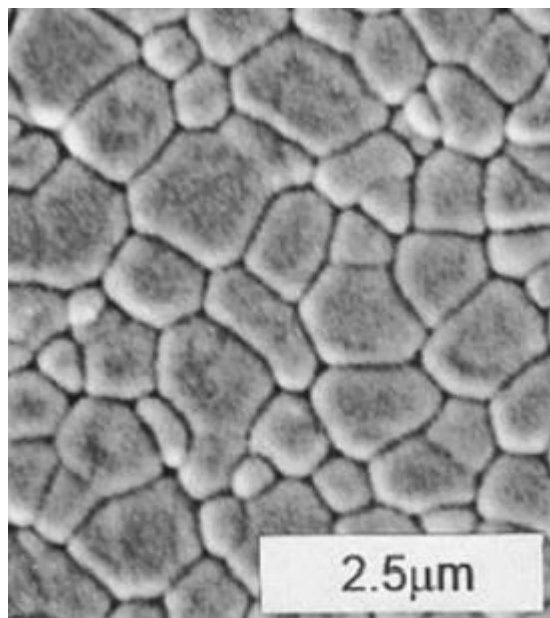
Figure 8. *Micrograph of Y-TZP (8).*

- **Partially stabilized zirconia - PSZ**

Partially-stabilized zirconia (PSZ), exhibits a microstructure that consists of t-precipitates within a c-stabilized zirconia matrix, as shown in Figure 9. It is usually obtained with the addition of magnesia (MgO), calcia (CaO) or Y_2O_3 (13). PSZ are the most widely studied and one of the toughest of the transformation toughened ceramics, it has a high strength and cracking resistance (15).

UNIVERSITAT POLITÈCNICA DE CATALUNYA
BARCELONATECH
Escola d'Enginyeria de Barcelona Est
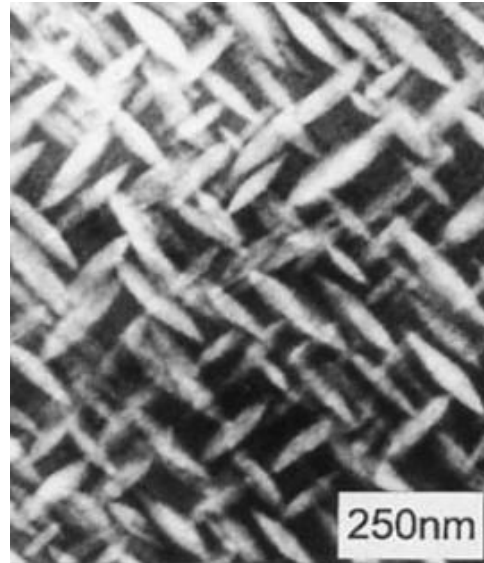
Figure 9. *Micrograph of t- precipitates in Mg-PSZ (8).*

Even though his good properties, the Mg-PSZ is unsuitable for dentistry applications because his high porosity and large grain size, which may lead to surface wear and large crack propagation (13).

- **Fully stabilized zirconia - FSZ**

Fully stabilized zirconia (FSZ) consists in an almost pure *c*-phase obtained at high concentration of stabilizers (more than 8 mol% Y_2O_3) (8). The microstructure presents a single-phase with large grains as shown in **Figure 10**.
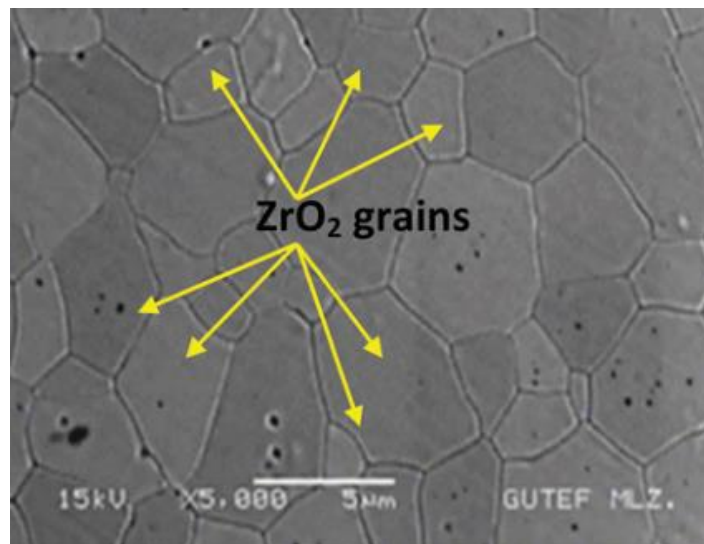
Figure 10. *Micrograph of fully stabilized zirconia with large grains of ZrO_2 (13).*

The increase in the amount of stabilizer improves its optical properties, improving the translucency of the material since the *c*-crystal exhibits greater volume than *t*-grains and are also more isotropic. However, strength and fracture toughness decreased because ZrO_2 stabilized in *c*-phase does not experience phase transformation (*t* -> *m*) (5). Therefore, the mechanical properties of FSZ are more influenced by the possible presence of defects induced during processing or conformation.

1.1.5.   Phase transformation

In 1975 the discovery of his toughening transformation gave the possibility of developing new applications for Zirconia, like biomedical applications (14). Before, pure ZrO_2 was not used for structural applications due to the transition from tetragonal (*t*-) to the monoclinic (-*m*) phase (*t* $\rightarrow$ *m*). This phase transformation its known to be a martensitic transformation and it implies a volume expansion that the material is not able to redistribute as depicted in **Figure 11** (2). In this sense, the expansion leads to stresses and induce cracks in the structures that decreases the mechanical integrity under service like condition.
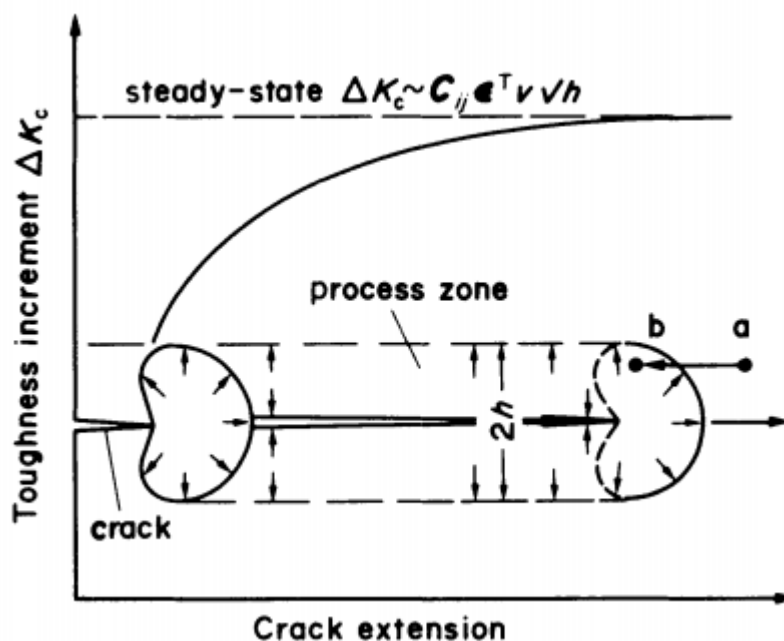
Figure 11. *Schematic diagram showing the development of the process zone with crack advance and the resultant toughness increment ΔK_c (16).*

This phase transformation can occur due to an ageing effect or spontaneously due to stresses in the material that generate cracks. These two methods of phase transformation are being studied and are explained in detail in the following points.

1.1.5.1. Toughening

Nowadays, the technology opportunities are available thanks to all the several major scientific discoveries that has allowed a better comprehension of this phenomenon. It is known that the $t \rightarrow m$ phase transformation can be supressed by total stabilisation in the *c*-form, but the most useful mechanical properties is a multiphase material called PSZ (2).

The $t \rightarrow m$ phase transformation usually occurs during the heating, cooling and sintering process and it involves a 3-5% volume expansion and induce stresses that creates microcracks. At the same time, this phase transformation creates a compressive residual stress and added to the energy spent on the phase transformation increase the fracture toughness when it occurs at the crack tip as shown in **Figure 12** [1, 2, 11, 16, 17].
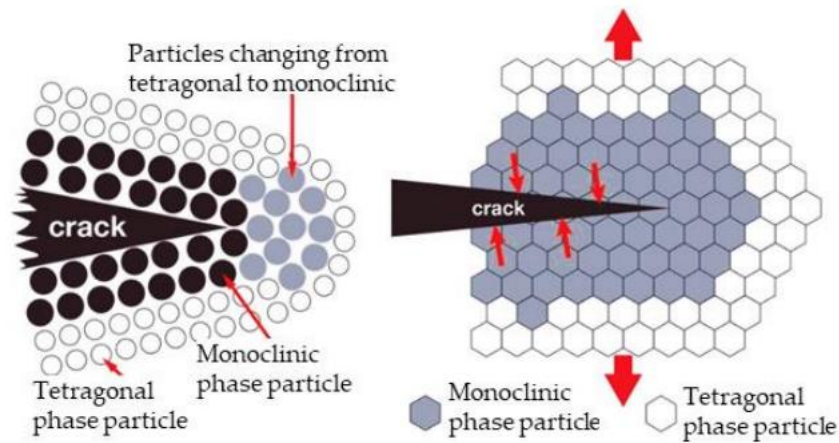
Figure 12. $t \rightarrow m$-phase transformation toughening mechanism in ZrO_2 (18).

The nucleation of the martensite plate of *m*-phase is controlled by the crystallographic orientation of the grains. Grains with their axis close to the free surface will be the first ones to transform. It initiates with the nucleation and growth of a martensite plate of *m*-phase through a habit plane, that involves a volumetric expansion and the generation of shear strain creating opposing stresses in the material, see **Figure 13**. Once the transformation has begun it starts to propagate by activating different correspondences, less favourable in terms of transformation strains accommodation. The opposite stresses generated by the first transformation can initiate the formation of another martensite plate with a plane close to the original martensite plain [18, 19].

UNIVERSITAT POLITÈCNICA DE CATALUNYA
BARCELONA**TECH**
Escola d'Enginyeria de Barcelona Est
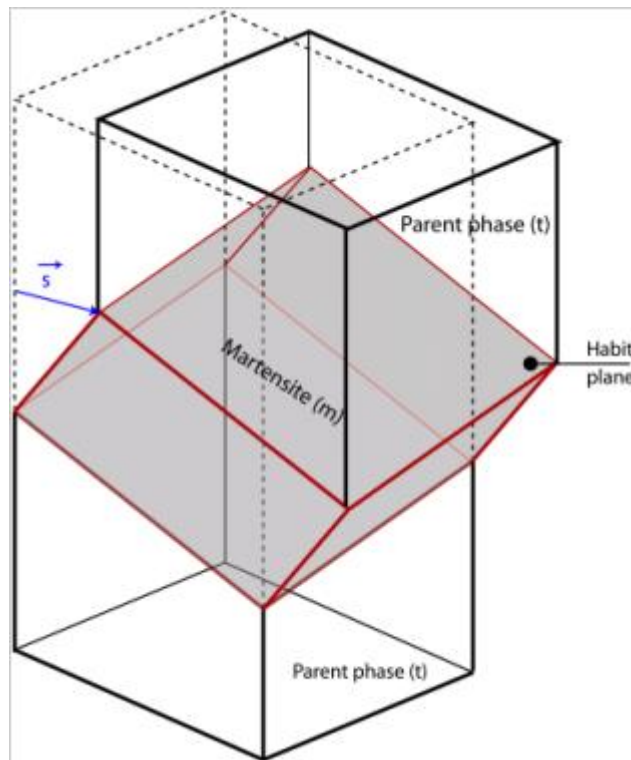
Figure 13 .*Schematic illustration of crystallographic between the t- (parent) and the m- (product) during the martensitic t →*
m phase transformation (20).

ZrO_2, like other materials, presents defects, the phase transformation will take place when the presence of a stress in a crack tip catalyses the $t \rightarrow m$-phase transformation. As has been mentioned above, this transformation involves a volume expansion of 3-5% and it is fast. This volume expansion is the responsible of the compressive residual stresses that close the crack and stop the propagation. This phenomenon is the responsible to enhance the fracture toughness of 3Y-ZrO_2. This mechanism is called transformation toughening and it is represented in **Figure 12** [16, 18].

1.1.5.2. Aging (Hydrothermal degradation)

The ZrO_2 suffers a low temperature degradation (LTD) also known as aging. This phenomenon causes a low and spontaneous $t \rightarrow m$ phase transformation at the surface of the material due to the presence of water. The LTD phenomenon is characterized by the following mechanism: in the initial stages and in the presence of water, the phase transformation takes places at low temperatures (65-300°C), where the degradation process causes a gradually phase transformation from the surface into the bulk of the ceramic. That trigger micro- and macrocracks develop by the expansion in volume associated with the phase transformation. Ultimately, LTD results in surface roughening and loss of mechanical properties [3, 20, 21].

UNIVERSITAT POLITÈCNICA DE CATALUNYA
BARCELONA**TECH**
Escola d'Enginyeria de Barcelona Est

In-vitro and *in-situ* studies have reported a wide variation in phase transformation susceptibility among different Y-TZP systems, which was shown to be dependent on several parameters. The complexity of such parameters on aging resistance on Y-TZP systems have not yet been fully understood (23).

Several hypotheses were proposed to explain the cause-and-effect relationship between the presence of water and the $t \rightarrow m$ phase transformation. Some studies highlighted that the surface chemisorbed water induces the separation of Zr-O-Zr bonds and allows the formation of Zr-OH. This results in stress corrosion located at the ZrO_2 grain boundaries. Otherwise, other researchers conclude that the phase transformation is caused by internal residual stresses associated with the diffusion of water radicals within the ZrO_2 lattice (22). The diffusion of the water species into the lattice results in a decrease of oxygen vacancies, that generates a change of lattice parameters causing internal stresses in the surface grains (20). This phenomenon results in the $t \rightarrow m$ phase transformation as represented in **Figure 14**.
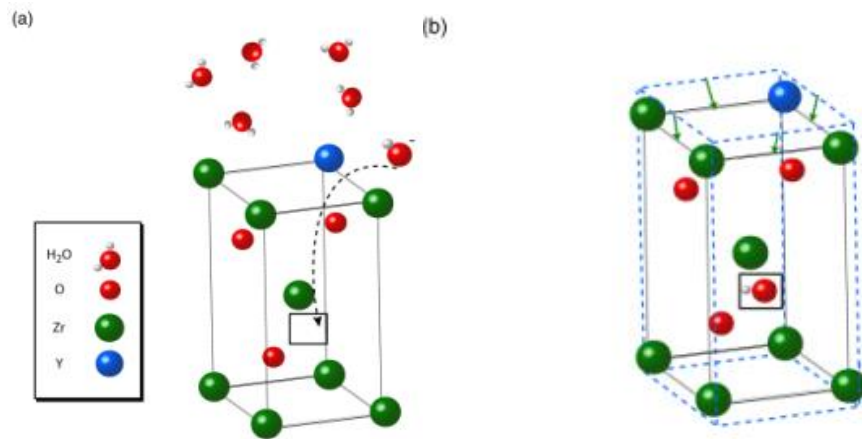
Figure 14. *a) Diffusion of water species into the lattice vacancies and b) the vacancies are filled generating a change in the lattice dimensions (20).*

This spontaneous phase transformation starts in the surface and progress by nucleation and growth process into the bulk material. The nucleation and growth of *m*-phase starts from grain boundary to the interior of one grain as shown in **Figure 15** (20).
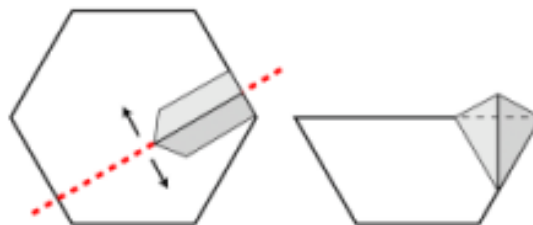
Figure 15. *Nucleation and growth of the m-phase in a grain, from the grain boundary to the interior (left and cross section on the right) (20).*

Simultaneously, other grains start to suffer the phase transformation and the ones that already has been transformed starts to growth. This transformed zone creates shear stresses in the enclosing *t*-grain at the grain boundary.

When the variants already transformed get to the gain boundary, the shear stress induce the material to be moved on the top side. If the adjacent grain cannot accommodate the stress, local tensile stress will appear at the grain boundary creating microcracks as shown in **Figure 16**.
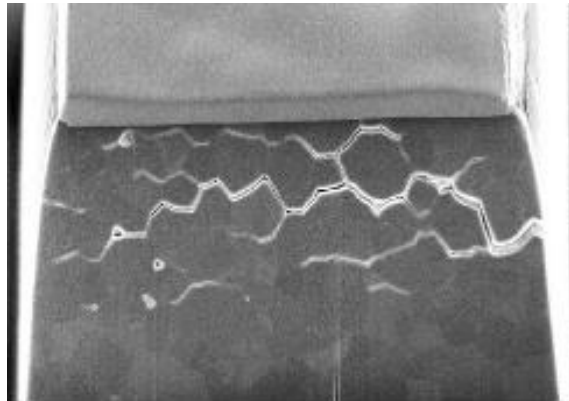
Figure 16. *Cross section image by Focused Ion Beam showing in detail the microcrack formed* (24).

The phase transformation will proceed in two different ways: (1) the cracks formed due to the stress allow water to penetrate the material causing the internal grains to begin to undergo LTD and (2) the stress generated due to the phase transformation will catalytically induce phase transformation in the neighbouring grains. These two ways cause the *m*-phase to increase rapidly as shown in **Figure 17** (23).
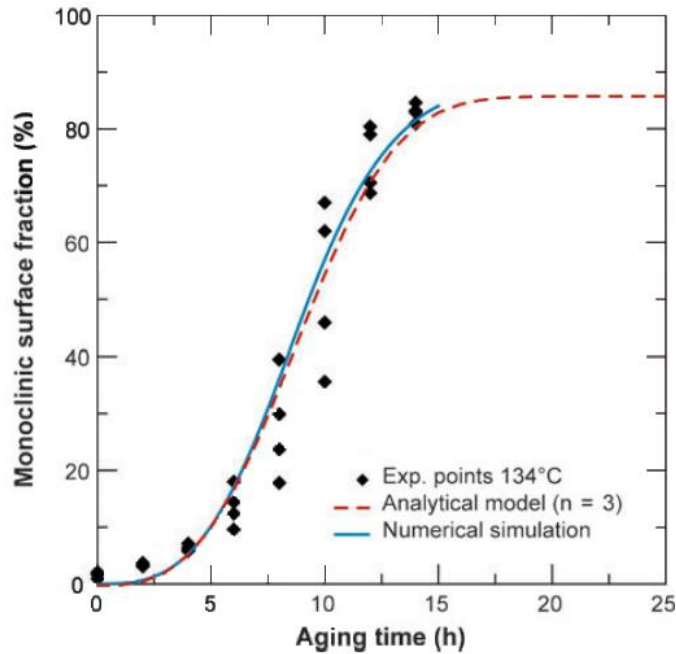
Figure 17. *Evolution of the m-phase vs time* (25)*.*

This problem can be reduced by doping ZrO_2 with different t-phase stabilizers. Using several stabilizers can enhance the LTD resistance and offers balanced properties. On the other hand, it is known that decreasing the grain size also reduces LTD (26).

Stabilizing the TZP with CeO_2 is an attractive alternative, the tetravalent nature of cerium maintains the charge neutrality of the system, there are not oxygen vacancies, and, consequently, the aging resistance is excellent (26).

Recent studies have shown that a composite with 85% Ce-/15% $Y-ZrO_2$ behave like a ductile ceramic, as it has a high hardness values and a fracture toughness higher than that the PSZ. Moreover, this material has a high percentage of Ce and because of that his LTD resistance is improved (27).

1.1.6.   Applications

ZrO_2 has become one of the most important ceramic materials due to his excellent mechanical properties and the recent discoveries, like the transformation toughening mechanism, this makes ZrO_2 the best option for a wide variety of applications. ZrO_2 is used as abrasive; as refractory paints for coating the surface of moulds, refractory bricks for furnaces or operating parts used in aggressive environments; as a gemstone for jewellery; and among others applications (28).

1.1.6.1. Biomedical applications

In the last decades, the use of material ceramics for the repair and reconstruction of damaged parts of the human body has been studied and it was demonstrated that they improve the quality of life.

When the materials are used in contact with the human body are called biomaterials, in this case bioceramics, and they are used as implants to repair or replace parts of the human body. Biomaterials must have biocompatibility, non-toxicity and also wear and fatigue resistance to withstand the thousands of cycles of stress generated by our body.

In the mid-eighties, ZrO_2 was introduced as an alternative to the alumina (Al_2O_3) femoral head for total hip replacement. ZrO_2 was expected to be an improvement on the higher fracture incidence of the Al_2O_3 implants. The material chose was $3Y-ZrO_2$. Up to date more than 500.000 femoral prosthetic heads have been implanted [26, 28].

However, even though some reports indicated that zirconia exhibited an exceptionally low fracture incidence, other heads produced by the same manufacturer had a disastrous performance. In 2001, more than 350 zirconia femoral heads from St. Gobain were retrieved from patients due to an unexpectedly high fracture rate cause by an accelerated LTD (30). One of the failures for $3Y-ZrO_2$ femoral heads is shown in **Figure 18.**

Figure 18. *Radiograph of fractured 3Y-ZrO$_2$ head* (29)..

UNIVERSITAT POLITÈCNICA DE CATALUNYA
BARCELONATECH
Escola d'Enginyeria de Barcelona Est

Nowadays, biomedical $3Y\text{-}ZrO_2$ has been studied, the problem of femoral heads was the beginning of a deeper studies to understand the behaviour of zirconia, especially the ageing. There is a trend today to develop $Al_2O_3\text{-}ZrO_2$ composites, that seems to be the future for femoral heads (31).

1.1.6.2. Dental applications

The dental implant market in recent years had undergone some changes and the $3Y\text{-}ZrO_2$ had become the best alternative to titanium, this is due to his superior aesthetic outcome, less plaque accumulation and lack of metal sensation. Most implants commercialised are made out of 3 mol. % $3Y\text{-}ZrO_2$ powder, other materials that are being used are $Al_2O_3\text{-}ZrO_2$ composites, among others. In **Figure 19** can be observed the geometry of this implants (14).

Figure 19. *Sraumann® implant* (32).

Although, ZrO_2-based ceramic implants are one of the most interesting materials, due to his phase transformation and good properties. In the physiological environment it suffers from LTD, and spontaneous phase transformation, which creates stresses inside the bulk of the implant and subsequently micro-cracks reducing the service like conditions of it.

This behaviour is known that is strongly affected and influenced by the grain size, initial powder, surface treatments and the stabilizer used. In this sense, as mentioned in section 1.1.1.2 12Ce- ZrO_2 do not suffer this degradation. One possible solution to enhance the LTD problem can be using a ZrO_2 composite material by mixing 12Ce and 3Y- ZrO_2 in different proportions, to achieve an implant that presents a better ageing resistance and good mechanical properties. Recent studies have shown that the most suitable composition is of around 85/15 12Ce/3Y- ZrO_2, as it presents a good compromise between the mechanical properties and the resulting material does not suffer practically (27).

1.2. Processing techniques

Currently, there are several ways to process ZrO_2. This material can be machined with the right tools but its high hardness presents complications. For this reason, in recent years other processing methods, such as additive processing, have been developed and researched. In this section some of these the different processing techniques will be explained and briefly compared.
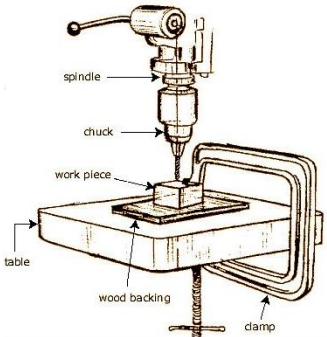
1.2.1.   Machining
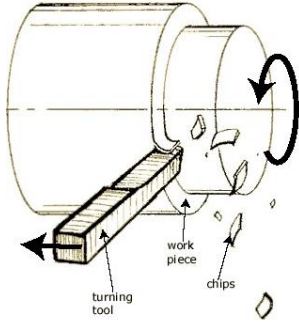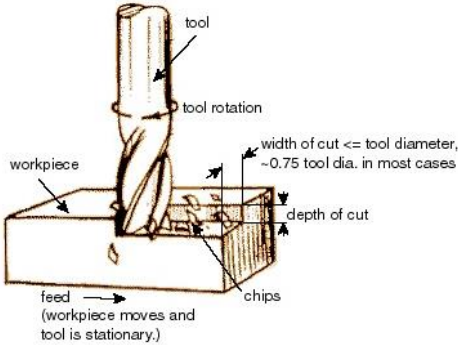
Machining is a manufacturing process that has been used for many years, especially for metalworking. It can be defined as the process of removing material from a workpiece using cutting tools. In the recent years, the search for materials with properties such as high specific strength, refractoriness and chemical stability has increased (33).

The common machining processes, although not the most suitable for dealing with ceramics materials, are commonly used as they give good results, but machining ceramics has always been challenging due to the brittle nature, high hardness, excess tool wear and edge breakage.

Traditional machining operations are classified into 3 principal processes: turning, drilling and milling. There are other operations such as, boring, sawing, shaping and broaching. Each type of process requires a specific tool [33, 34]. The principal common machining tools are explained in detail in **Table 1**.

Table 1. *Types of machining tools.*

Machining Tool	Description	Scheme
Drilling	In this process holes are created through a twist drill. This tool has a pointed end which is responsible for making the hole. In this process the drill enters the workpiece and cuts a hole which has the same diameter as the tool used. A schematic representation of the machine can be found in **Figure 20** (34).	**Figure 20**. *Drilling machine* (34).

Turning	This process is a lathe operation, in this process material is removed from the outside of the workpiece, i.e. from its outer diameter, using a cutting tool, as show in **Figure 21**. This operation is carried out on a lathe which is a machine where the workpiece is adjusted and is rotated while the tool is stationary, with this method is possible to cut in a precise way the unwanted parts from the piece.	**Figure 21**. *Turning process* (34).
Milling	This process has a high degree of freedom, this makes it less precise than turning processes. The workpiece is the material already shaped; it is secured to the fixture. The cutter has sharp teeth and it rotates at a high speed as depicted in **Figure 22** (34).	**Figure 22**. *Milling process* (34).

Conventional machining processes are not very suitable for working with ceramics, due to the properties of these materials which cause tool wear (36). Even though they present these problems, ceramic materials can be processed by non-traditional machining (NTM), whose material removal mechanism primarily take place due to abrasion, some of these techniques are explained as examples below (33).

- **Rotatory ultrasonic machining (RUM):**
  This technique is a NTM that combines diamond grinding with ultrasonic vibrations as seen in **Figure 23.** A hollow tool and metal-bonded diamond abrasives are used in this process. The hollow tool is vibrated ultrasonically in an axial direction, through the centre of which, coolant is allowed to carry abraded particles away from the machining zone, preventing the congestion of the tool and keeps the tool cool. The cutting parameters on the RUM are spindle speed, feed rate, cutting depth, amplitude and frequency of ultrasonic vibrations (37).

UNIVERSITAT POLITÈCNICA DE CATALUNYA
BARCELONA**TECH**
Escola d'Enginyeria de Barcelona Est
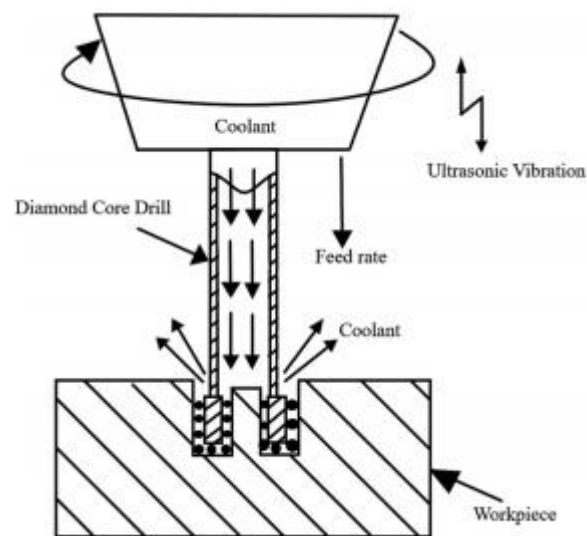
Figure 23. *Rotatory Ultrasonic Machining* (37)*.*

- **Laser machining (LM):**

  This is a non-contact type of NTM that uses a highly collimated laser beam which strikes the sample with high energy such that the temperature of the workpiece exceeds its boiling point, resulting in vaporization and ablation of work material as shown in **Figure 24** (36).
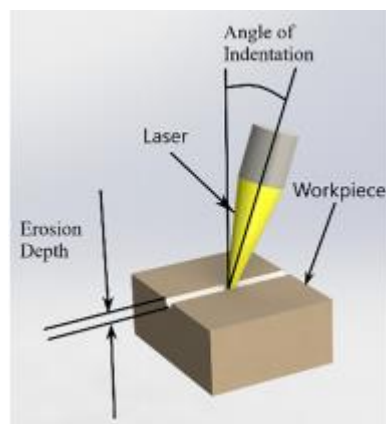
Figure 24 .*Laser Machining* (36)*.*

The main mechanisms involved in the material removal process are surface melting, vaporization, chemical dissociation, plasma formation, ablation among others. The parameters that affect the process are: *type of laser used*, *laser operation* (continuous or pulsed), *power density* and *time period of the laser pulse*. Pulsed laser in laser machining of ceramics has led to the observation that it provides better quality finish (38).

UNIVERSITAT POLITÈCNICA DE CATALUNYA
BARCELONA**TECH**
Escola d'Enginyeria de Barcelona Est

There is another technique similar to LM called Laser Assisted Machining (LAM). The main differences between these two techniques are: the temperature operation, in LAM generally the temperature operation is around the recrystallization temperature, and that LAM uses a secondary-in-process material removal process. The material removal takes place through a quasi-ductile mechanism. It has been observed that LAM gives a better surface finish and lesser cutting forces compared to traditional processes [36, 37].

1.2.2.   Additive Manufacturing process

Currently, the 3D printing technology is growing interest in the processing industry due to this methodology leads produce complex shapes and reduce considerable the production costs. In this regard, this technology is quite new for developing ceramic based materials. In this regard, the direct ink writing (DIW) technology is widely employed to 3D printing ceramic materials, it consists on the extrusion of viscous ceramic pastes. In this sense, one of the main key parameters are the rheological properties in order to be able to (**Figure 25**). In this regard, the rheological properties are one of the most important parameters to prevent the deformation of the printed sample, several methods are used to control this parameter, such as modification of the pH, or addition of additives among others (39).
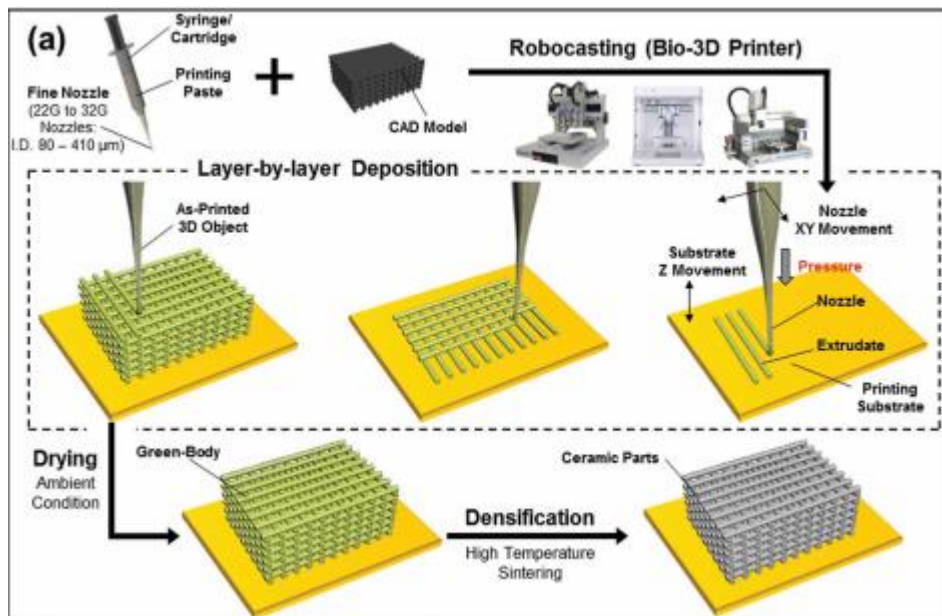
Figure 25. *Schematic diagram of the DIW technique* (39).

This technique is used to build-up the ceramic green body, that afterwards is should be sintered to achieve the final ceramic properties. This technique is nowadays widely in the production of 3Y-ZrO$_2$ parts (40).

In order to compare the two techniques explained in this section, **Table 2** has been created to summarise the advantages and disadvantages of each manufacturing method.

Table 2. *Advantages and disadvantages of the manufacturing techniques* (39).

Method	Advantages	Disadvantages
Machining	• Geometry: As solid block of the material is used to make the desired geometry. As no sintering is required, the resulting part will not change in size. • Size: With these techniques, part of different sizes can be produced without significantly affecting the production time.	• Tool wear: Due to the high hardness of the ceramic materials, the tools are subject to a wear and can break faster. • Edge brakeage: Some ceramic material may suffer from cracking at the corners due to the brittleness of these materials.
Additive Manufacturing	• Material efficiency: AM techniques uses directly the ceramic feedstock more efficiently than other conventional subtractive manufacturing techniques by building the parts layer by layer. • Resource efficiency: AM does not require additional resources like fixtures, cutting tools, coolants in addition to the main machines. • Part flexibility: The parts manufactured can have complex features and can be made in a single piece. In addition, it is possible to build a single part with different mechanical properties. • Flexibility: The quality of the parts depends on the process rather than operator skills. This makes the production easier to synchronise with costumer demand.	• Size limitations: Due to the low strength of the material used for printing, liquid polymer or plaster, these techniques may produce large parts, but it is difficult and the time to produce them would be very long. • Imperfections: Ceramic parts produced using AM techniques often have a rough surface finish. This is due to plastic beads or large-sized powder particles stacked on each other. • Cost: AM equipment is expensive. The average price for an average 3D-printer is 2.500€ up to 600.000 €. Excluding costs of materials and accessories.

UNIVERSITAT POLITÈCNICA DE CATALUNYA
BARCELONATECH
Escola d'Enginyeria de Barcelona Est

1.3. State of art

To analyse the state of the art of the topics studied in this bachelor's project, the ISI Web of Knowledge and Scopus has been used as a Data Base. Both show the number of manuscripts related to a certain keyword related with the subject investigated here. In this research, some topics related to the project were searched from the last 20 years (2000 to 2020) in order to see the novelty of this research. First of all, the impact of *ZrO$_2$ based dental implants* in recent years was sought (**Figure 26**). As you can see, since the year 2000 the research on ZrO$_2$ based dental implants growth exponentially and becomes an important material in this field.
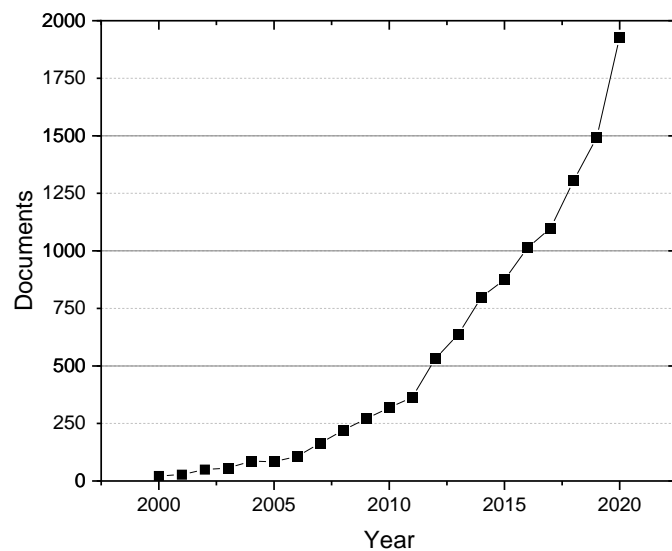
Figure 26. *Representation of the published paper related with ZrO$_2$ dental implants.*

To find out how many of these articles were related to 3D printing or machining of implants, another search was carried out with the following keywords: *ZrO$_2$, dental implant and 3D printing or cutting*. As it is shown in **Figure 27** there are few related papers to 3D printing and they are very recent. In the case of machining, there are more documents related but most of them are non-traditional machining, only one article has been found that talks about traditional machining. It can be also observed that since the appearance of the 3D printing related articles, these have become more popular. It is also important to note that all these articles talk about 3Y-ZrO$_2$.
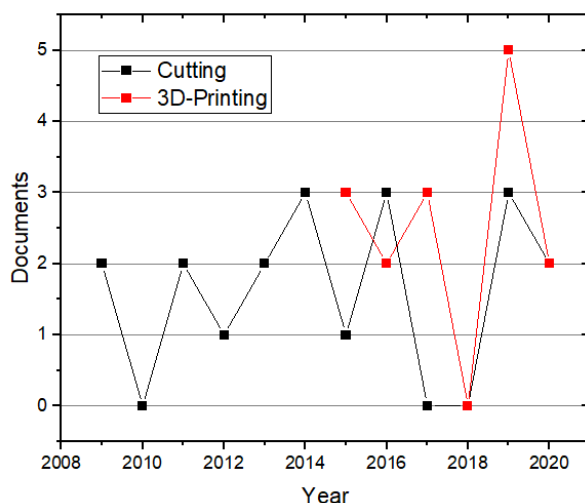
Figure 27. *Representation of the published paper related to 3D-Printing and cutting of dental implants.*

After studying the state of art in manufacture techniques, the 3 materials that will be studied along this bachelor's degree have been searched to verify its impact and importance. The documents related to 3Y-ZrO$_2$ have increased considerably during this period due to its multiple applications and the search of improvements to avoid LTD. This may be related to the small increase in the articles related to 12Ce and 12Ce/3Y -ZrO$_2$ since ceria or cerium oxide (CeO$_2$) seems to reduce the effect of hydrothermal degradation. As it is depicted in **Figure 28**, the amount of published papers for the 12Ce-ZrO$_2$ and 12Ce/3Y-ZrO$_2$ decreases considerably doing the research presented behind this bachelor's degree project, making it new and also at the same time interesting for the scientific community.
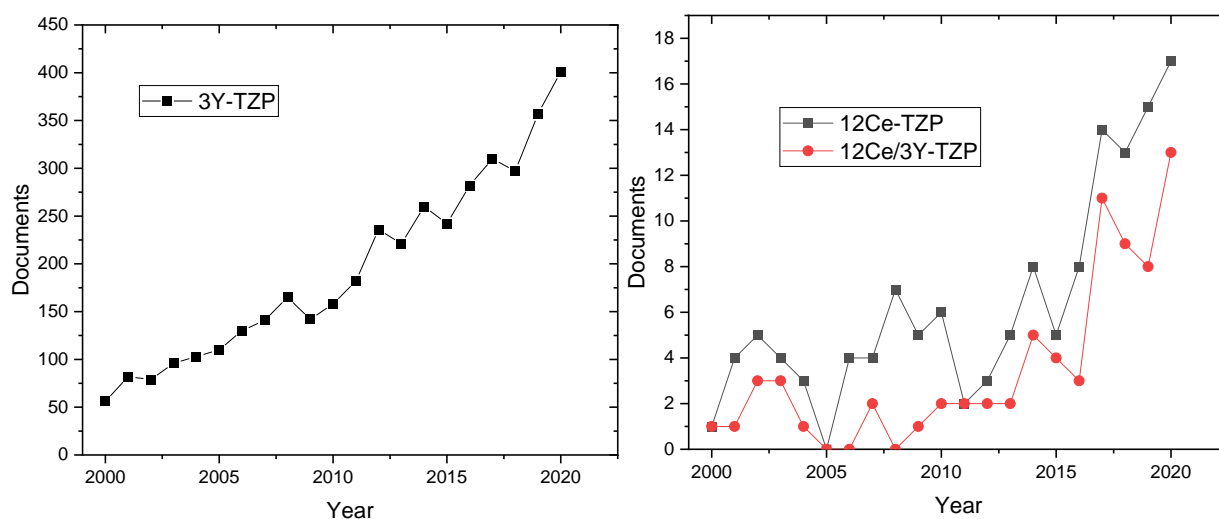
Figure 28. *Representation of the published paper related to 3Y-TZP (left), and 12Ce-TZP and 12Ce/3Y-TZP (right).*

Among the articles found there will be commented the articles that talk about the $12Ce/3Y-ZrO_2$ and dental implants, as well as two articles related to the implant manufacturing process, one from 3D printing and the other from cutting.

M. Turon-Vinas, J.J. Roa, F.G. Marro, M. Anglada. Mechanical properties of $12Ce-ZrO_2/3Y-ZrO_2$ composites (2015) (27)**.**

This paper is an investigation about the mechanical properties of different composites made out of $12Ce/3Y-ZrO_2$. In addition, the composite (85% $12Ce-ZrO_2$/ 15% $3Y-ZrO_2$) with better compromise between mechanical properties and resistance to LTD, has been processed at different temperatures. This article is the precedent to begin this investigation since the composite that have been studied is a nice option to be used in dental applications.

R.B. Osman, A.J. van der Veen, D. Huiberts, D. Wismeijer, N. Alharbi. 3D-printing zirconia implants; a dream or a reality? An in-vitro study evaluating the dimensional accuracy, surface topography and mechanical properties of printed zirconia implants and discs (2017) (41)**.**

In this article the dimensional accuracy, surface topography of a 3D-printed zirconia dental implant is evaluated together with an evaluation of the mechanical properties of printed zirconia. In this article they do a research similar to that which will be carried out in this Bachelor's degree project, but in this article is focused on the $3Y-ZrO_2$.

H.B. Lim, T. Dongxu, K.J. Lee, W.S. Cho. Green and hard machining characteristics of zirconia-alumina composites for dental implants (2011) (42)**.**

This article discusses the investigation of ceramics used to make dental implants, and studied the machining of these ceramics on a computer numerical control lathe for an $Al_2O_3-ZrO_2$ composite under different machining conditions. The method used in this article is similar to the one intended to be used in this project, but the materials and tools used are different.

T. Murakami, A. Nakahira, T. Kudou, T. Matsuhita, T. Honma. Fabrication and evaluation of high performance $12Ce-ZrO_2/3Y-ZrO_2$ composites for an implant (2006) (43)**.**

In this article 3 composites of $12Ce/3Y-ZrO_2$ are evaluated and it is concluded that by having a composite containing a 10 and 20% of $3Y-ZrO_2$ his LTD resistance is increased, also the mechanical properties are analysed and the composite gives values close to 10 GPa in hardness and 7-8 $MPa \cdot m^{1/2}$ in terms of indentation fracture toughness. This article reaffirms the motivation to carry out this project as this composite is a very interesting material to replace $3Y-ZrO_2$ implants.

UNIVERSITAT POLITÈCNICA DE CATALUNYA
BARCELONATECH
Escola d'Enginyeria de Barcelona Est

After analysing all the articles related to the techniques that will be used in this final degree project, as well as analysing the articles that talk about the composite that will be evaluated. It can be concluded, that this makes this research innovate and cutting-edge.

UNIVERSITAT POLITÈCNICA DE CATALUNYA
BARCELONATECH
Escola d'Enginyeria de Barcelona Est

2. Objectives

The long term goal behind this bachelor's degree project is to compare the manufacture process of an implant between 3D printing and traditional machining process, and study how it performs by using three Zirconia-based materials. Especially with the 12Ce/3Y composite.

To achieve this purpose, three Zirconia based ceramic materials were characterized. 3D printed and compression moulded samples will be microstructurally and mechanically characterised and compared, and the effect of LTD on them will be studied to observe the changes in their mechanical properties. In order to compare the two manufacturing methods, the final shape of the implant will be observed. An attempt will be made to machine the material using traditional machining techniques and to 3D print it using the direct ink writing (DIW) technique.

In order to fulfil the main objective of this project, <u>secondary objectives</u> have been set to be fulfilled:

a. Characterize the powders to study the viability of 3D-printing.
b. Characterise the mechanical properties of the three materials before and after the Hydrothermal degradation test. And compare the results between samples made by Cold Isostatic Pressing and 3D printing.
c. Attempt to print the implant and try to machine it with traditional techniques.
d. Compare the printing results between the different materials and analyse the feasibility of printing the implant for use.

3. Experimental methodology

3.1. Sample preparation

The powders used in this study were 3Y-TZP (Zirconia with 3% mol Y_2O_3) and 12Ce-TZP (Zirconia with 12% mol CeO_2) commercia powders from Tosoh Corporation (TZ-3YSB-E) and Daiichi Kigenso Kagaku Kogyo of Japan, respectively. To obtain the mixture of 85/15 12Ce/3Y-TZP the two powders were wet ball milled with ethanol. This composition was chosen as the appropriate due to Turon-Vinas *et al.* (27) found that this ratio enhances the hydrothermal degradation and the fracture toughness by slightly reducing the hardness for the resulting material.

The powders were uniaxially pressed at 14 MPa for 3Y-TZP, 10 MPa for 12Ce-TZP and 8 MPa 12Ce/3Y-TZP, and by cold isostatic pressing (CIP) at 30 MPa using the CIP-30MA from MTI Corporation (**Figure 29**).

Figure 29. *Cold Isostatic Pressing machine used in this bachelor's degree project.*

UNIVERSITAT POLITÈCNICA DE CATALUNYA
BARCELONA**TECH**
Escola d'Enginyeria de Barcelona Est

3.1.1.   *Conforming methods*

Sample were also processed by the methods that will be compared in this study, machining and 3D-printing.

a.   *Milling*

The initial idea was to try to manufacture these samples according to the implant design, see **Annexe B1**. But due to the lack of time, the hardness (*H*) of the material and the small size of the implant, a facing and turning operation were made to study the effect of this operations in the material surface.

The samples used for machining were made with a uniaxial pressing machine, this machine could make bar-shaped samples, which were necessary to hold the sample on the lathe. The lathe used was a CNC lathe ST from *Pinacho* as depicted in **Figure 30**. In a study that discusses the machining of ZrO_2 composites, PCD (polycrystalline diamond) tools were used (42), but in the absence of these tools, in this bachelor's degree work it was used an insert (CNMG120408 SM, see **Figure 31**).

Figure 30. *CNC Lathe ST (Pinacho)*

Figure 31. *Tools used on the lathe CNMG120408 SM.*

After the uniaxial conformation, it was seen that the samples could not be machined in the lathe due to their geometry. Then was decided to try to machine the samples in the milling machine to observe the material behaviour and analyse it surface after the milling. For this purpose, a CNC milling machine MC 600 from *Lagun* was used, the tool used was a HMP HSS-Al Denmark end mill G-122-003, flatted shank with a diameter of 3 mm and 2 flutes. The test done consist on several passes of the milling through the material surface, in each cycle the depth was increased by 0.1 mm, during all the process the piece was refrigerated with coolant. The parameter used for this operation were, speed of 1000 rpm and a feed rate of 200 mm/min.

b. Direct-ink writing

Before starting the printing process, it is necessary to produce the ceramic paste. Pluronic F-127® from SIGMA-ALDRICH is used as a polymeric matrix, and the 3 zirconia-based ceramic materials as ceramic charge in order to produce the desired ceramic ink. The ceramic ink consists on a mixture between, distilled water, Pluronic F-127® and ceramic powder in the right proportions.

This type of paste is currently being widely used in many fields due to its good rheological properties and it is also a biocompatible hydrogel which makes it ideal for biomedical applications.

First of all, to make the ceramic ink it is necessary to prepare the hydrogel. In this sense, Pluronic F-127® is mixed with distilled water at 3500 rpm during 5 minutes in the *SpeedMixer*, see **Figure 32**. Once this is done, the mixture has to be left at 4⁰C for 48 hours before preparing the ceramic paste in order to remove the bobbles, which can act as printing defect, generated during the mixing process.

UNIVERSITAT POLITÈCNICA DE CATALUNYA
BARCELONA**TECH**
Escola d'Enginyeria de Barcelona Est

Figure 32. *SpeedMixer*

Then the paste has to be prepared, for each of the materials the ceramic charge was different, for the 3Y-ZrO$_2$ a load of 7.,5% was used, for the 12Ce-ZrO$_2$ a load of 68% and for the composite a load of 68.5%.

The total weight of the ceramic paste was 20g. To prepare it, the % of ceramic charge was weighed and the rest was filled with Pluronic F-127®. Once the mixture was ready, it has to be introduced in the speed mixer for 30 seconds at 3500 rpm. It is important to be sure that not conglomerates are left in the paste as they can seal the nozzle, if conglomerates are observed, it should be put in the *Speedmixer* again with the same conditions. This step has to be repeated until they disappear.

To work with DIW processes it is very important to control the parameters. Is important to control the velocity of the movements, the infill of the samples, the printing pattern, among others. All these parameters were controlled through the software called *Slic3r*, see **Annexe A1**. The geometry of the implant was designed in *Solidworks*, **Annexe A2**, and uploaded to *Slic3r* to generate the code to use it in the printer.

Before starting printing of the implant, squares of 10x10x10 cm dimensions were printed in order to compare the properties of the printed material with the one processed by powder compression. In addition, test could be carried out to see how the material was printed and which ceramic charge should be used. The properties of the printing process followed in this Bachelor's project are summarized in **Table 3**.

Table 3. *Properties of the print process.*

Speed for print moves								
Infill	**Partner**	**Perimeters**	**Small Perimeters**	**Infill**	**Solid infill**	**Bridges**	**Gap infill**	**Speed for non-print moves**
100%	Rectilinear	3 mm/s	3 mm/s	3 mm/s	3 mm/s	5 mm/s	3 mm/s	30 mm/s

The nozzle used in this printer has a diameter of 0.52 mm.

3.1.2. Sintering process

The sintering process is a key step in densifying the green part to achieve the desired mechanical and microstructural properties. The oven used to do this process was a *Nabethern* furnace, see **Figure 33**.

Figure 33. *Nabethern furnace*

Three different thermal treatments (TT) were carried out depending on the material, for 3Y-ZrO$_2$ the maximum temperature reached was 1450°C for 1 hour (**Figure 34a**), for the 12Ce-ZrO$_2$ the temperature was 1450 $^{\circ}$C for 2 hours (**Figure 34b**) and finally for the composite material, the maximum temperature was 1550 $^{\circ}$C for 2 hours (**Figure 34c**) (27). The heating and cooling rate for all the three different TT was held constant and equals to 3 $^{\circ}$C·min^{-1}.

UNIVERSITAT POLITÈCNICA DE CATALUNYA
BARCELONA**TECH**
Escola d'Enginyeria de Barcelona Est

In addition, three sample made by CIP once polished were thermally etched to reveal the grain boundary and be able to quantify the grain size. This treatment was similar to the sintering but the maximum temperature was 150 °C lower for each material.
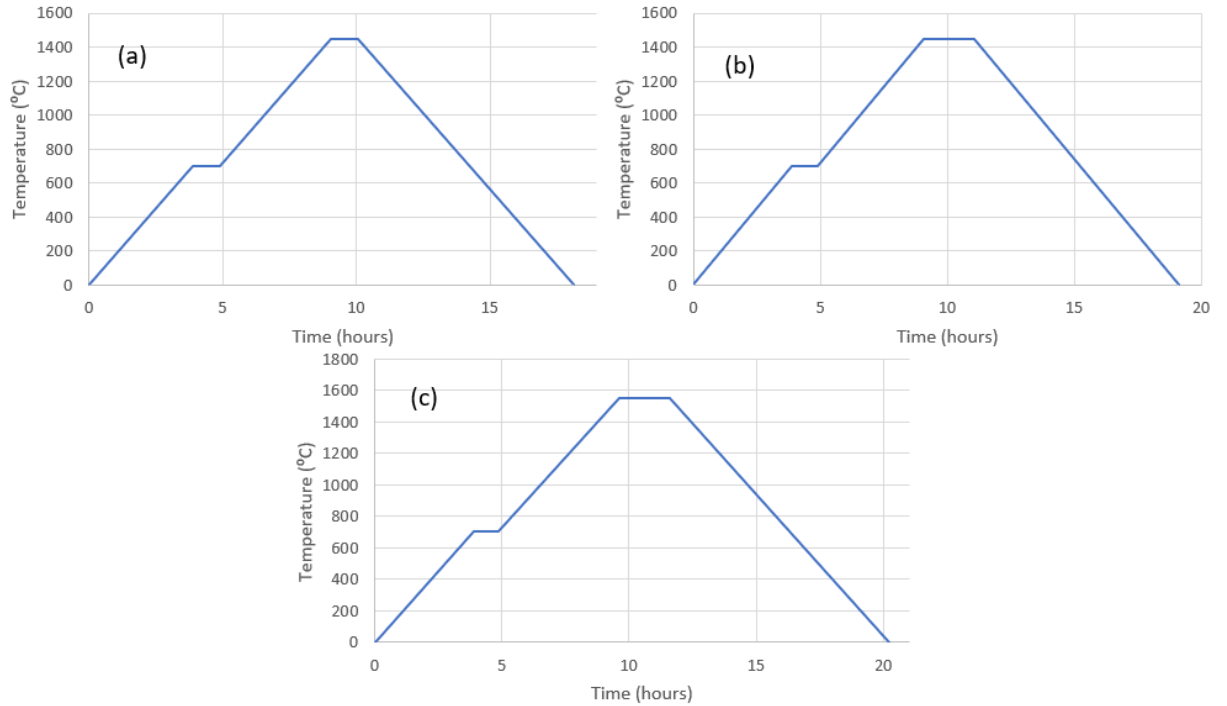
Figure 34. *Sintering process for (a) 3Y-ZrO$_2$, (b)12Ce-ZrO$_2$ and (c) 12Ce/3Y-ZrO$_2$ samples.*

3.1.3. Polishing methods

Prior the microstructural and mechanical characterization, the samples were polished until reach mirror-like surface by using different water-based diamond slurries (30 μm – 6 μm – 3 μm) with a final step of diamond suspension of 1 μm. In **Figure 35** it is shown the polishing machine as well as the polishing cloths, moreover in **Table 4** are summarized the polishing steps.

UNIVERSITAT POLITÈCNICA DE CATALUNYA
BARCELONA**TECH**
Escola d'Enginyeria de Barcelona Est
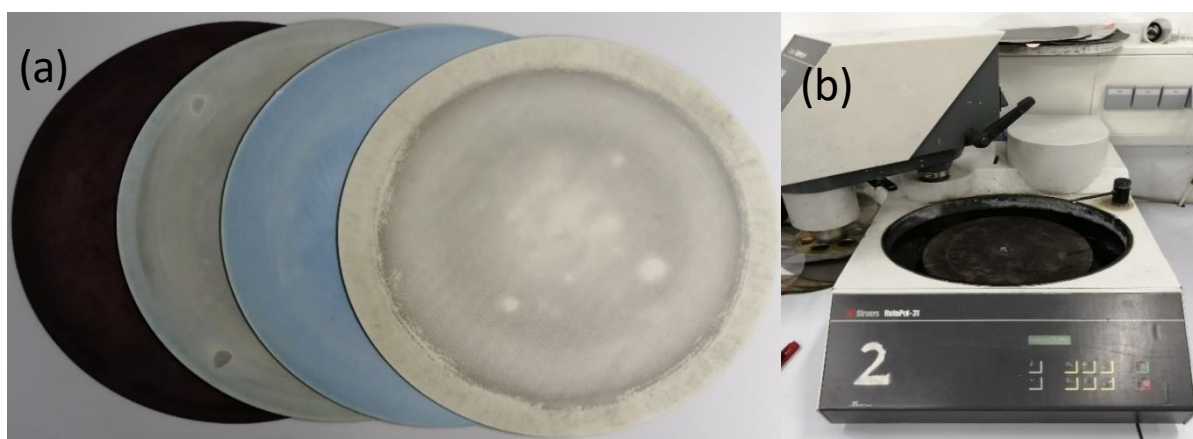
Figure 35. *(a) Polishing cloths and pastes, (b) Polishing machines.*

Table 4. *Summary of the polishing steps*

Step	1	2	3	4	5	6
Polishing speed	300	300	150	150	150	150
Time	10	10	5	10	15	20
Polishing cloth	Sandpaper P:1200	Sandpaper P: 220	Polishing cloth	Polishing cloth	Polishing cloth	Polishing cloth
Suspension	Water	Water	30 µm	6 µm	3 µm	SiO_2

3.2. Microstructure characterization

In this section the different techniques used to microstructurally and mechanically characterise the material are briefly explained.

3.2.1. Laser Diffraction

Laser diffraction (LD) measures the particle size distributions by measuring the angular variation in density of light scattered as a laser beam passes through a dispersed particulate sample. The large particles scatter light at small angle and small particles scatter light at large angles. The angular

scattering intensity data is analysed to calculate the size of the particles responsible of this scattering pattern. The particle size is reported as volume equivalent sphere diameter (44).

The equipment used in this Bachelor's project was the Masterseizer 3000, Malvern, and is shown in **Figure 36**. This technique was carried out to determine the particle size distribution of the powders in order to find out if it was possible to print. The study was made with the powders in a water suspension. First mixed at 3500 rpm and then mixed with the same rpm but with the ultrasounds activated.

Figure 36. *LD equipment.*

3.2.2. Density

The density of the CIP and the 3d-printed samples has been determined by Archimede's principle, using a balance from Mettler Toledo, model xs3035 shown in **Figure 37**. This principle states that a fluid immersed in a fluid experiences an upward force, proportional to the density of the fluid and the volume of the body. The density value can be determined using the **Ec. 1**. The auxiliary fluid used was water, so the ρ_0 is equal to $1\frac{g}{cm^3}$.

$$\rho = \frac{A}{A-B} * (\rho_0 - \rho_L) + \rho_l; \ \rho_L = 0,0012 \ \frac{g}{cm^3} \tag{1}$$
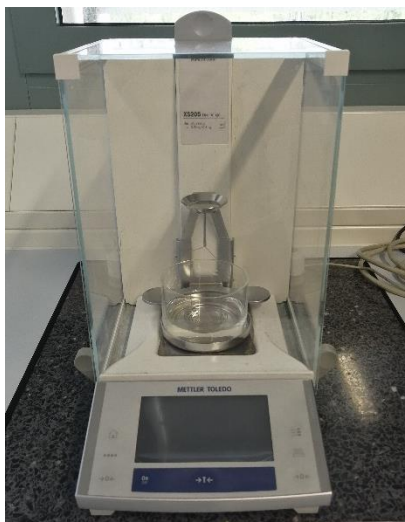
Figure 37. *Model xs3035, Archimede's method equipment.*

3.2.3. *Optical Microscopy*

The optical microscopy (OM) is an instrument that uses visible light passing through a series of lenses to magnify the image of observed sample. The samples are placed on a mobile platform which can be illuminated from below or from above depending on the type of microscope being used. A group of lenses allows the user to view images at different magnifications. In this Bachelor's project an Olympus BX53M optical microscope was used, it has 4 different objective lenses at the following magnifications: 5x, 10x, 20x and 50x. This microscope also has a camera attached to it which allows the images to be displayed on a computer. In **Figure 38** an image of the microscope can be seen. This equipment was used to observe the indentations and measure the cracks.

Figure 38. *Olympus BX53M optical microscope.*

3.2.4. Scanning Electron Microscopy

Scanning electron microscope (SEM) is a high-resolution imaging technique for investigation of the surface topography and morphology of samples. It consists on cathode that contains a tungsten filament which excites a beam of electrons though an anode. This beam is aligned and focused by three electromagnetic lenses. Finally, when it reaches the sample, the information of the interaction between the beam and the sample is collected by three different detectors, in the **Figure 39** a scheme of the SEM can be seen. Each one of them gives a specific information about the sample.

The secondary electrons (SE) provide a more detailed surface and topography information, they are generated by the inelastically interaction of the electrons of the beam with the atoms of the sample.

Backscattered electrons (BSE) show differences in atomic number (the higher the atomic number, the brighter appears in the image). They are electrons from the beam that elastically interact with those atoms of the sample. They come from a deeper part of the surface.

X-Rays are generated by the atoms in the sample as a result of an excitement and posterior relax of an electron from an inner shell to an external one. These rays give qualitatively information about the elements found in the samples. This technique is known as EDX.

All the SEM equipment must be in high vacuum to avoid unexpected interactions. In this Bachelor's project, it is going to be used to microstructurally characterize the surface of the different materials and it will also be used to measure the diagonal and the cracks of the microindentation to calculate the indentation fracture toughness. The model used in this bachelor's project is the "Phenom XL" shown in **Figure 40**.

UNIVERSITAT POLITÈCNICA DE CATALUNYA
BARCELONA**TECH**
Escola d'Enginyeria de Barcelona Est
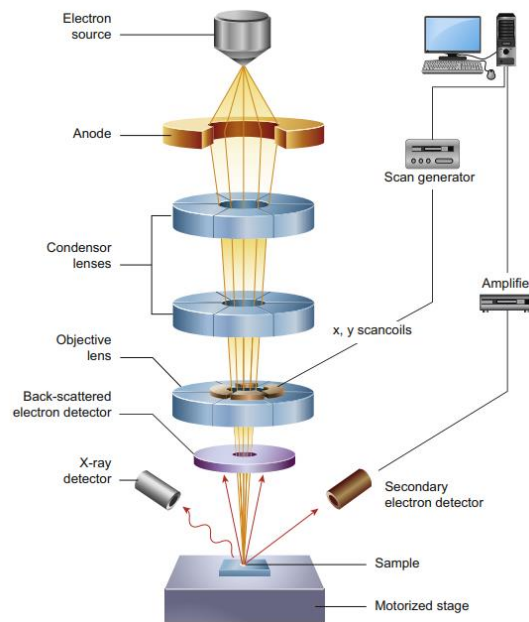
Figure 39. *SEM column scheme* (45).

Figure 40. *Phenom XL*

3.2.5. Field Emission Scanning Electron Microscopy

The Field Emission Scanning Electron Microscopy (FE-SEM) is a dispositive based on the same principle as the SEM. The main difference between these two techniques is that FE-SEM generates the electrons in an electric field, with this method is obtained an image with better resolution. This technique was used to observe the grain boundaries, as the SEM could not provide an image with a good resolution to determine the size of the grains. The FE-SEM images were taken using a Zeiss Neon 40 Cross-Beam.

In order to obtain the grain size values, the software ImageJ was used. This program allows the user to perform measurements on an image. In this Bachelor's degree the program will be used following the standard, ***ASTM-E112***, to make a linear intercept method (LIM) to obtain the grain size value (46). In the **Figure 41**, is shown an example of the procedure. First, lines are drawn on the image, then the grain boundaries that intersect with the line are counted. In this Bachelor's degree, two images were measured for each sample and 16 lines were drawn in each one.
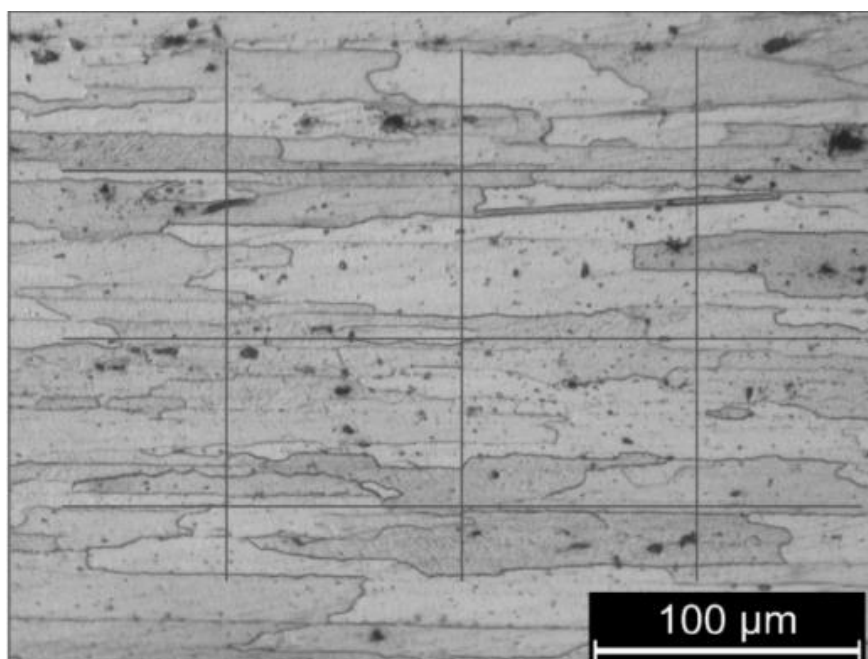
Figure 41. *Example of the linear intercept method* (47).

3.2.6.   X-Ray Diffraction

X-Ray Diffraction (XRD) gives information about crystal phases hold in powder or in the studied material. X-rays are generated in a cathodic tube; a tungsten filament is heated and it accelerates electrons to a copper cathode. The collisions between the electrons and the copper cathode results in inner shells ionizations that produces X-rays. This X-rays interact with the sample and diffract other X-rays only when a constructive interference between two atomic layers occur. In order to change the incident angle of the X-ray beam a goniometer rotates the sample.

In this Bachelor's project, the device used was a "Bruker D8 Advance" X-ray diffractometer, with the following conditions: $20 < 2\theta < 100^{o}$ using a constant step size of $0,02^{o}$. The device is shown at the **Figure 42**. This equipment was used to study the crystalline phases of the powders and later the phases of the samples after LTD.

UNIVERSITAT POLITÈCNICA DE CATALUNYA
BARCELONA**TECH**
Escola d'Enginyeria de Barcelona Est
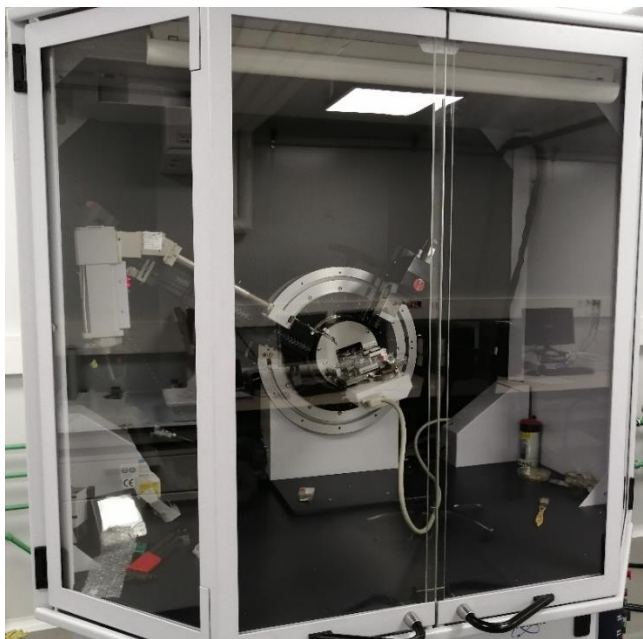
Figure 42. *Bruker D8 Advance.*

3.3. Hydrothermal degradation

This test was used to observe the behaviour of the 3 ZrO_2 based materials after been exposed to the LTD. An accelerated degradation with water steam at $134\,^{\circ}C$ and 2 bar of pressure was performed in a Micro 8 (selecta) for 10 hours (see **Figure 43**).

Figure 43. *Micro 8 (selecta)*

Once the degradation test was finished the samples were mechanical characterized with Vickers hardness test to register the changes in hardness and fracture toughness. Moreover, it was also

performed a XRD study to understand the changes on the mechanical properties by studying the changes in the crystallographic phases.

3.4. Mechanical characterization

3.4.1. Vickers hardness

Hardness (*H*) defines the ability of a material to withstand local plastic deformation. Indentation methods consist of pressing a sample material and measuring the response, this test is widely used for mechanical characterization of metals, ceramics and coating materials.

Vickers hardness (HV) test is one of the most commonly used hardness measurements methods, this test is done at the micrometric length scale, therefore is it also known as microindentation test.

It uses a diamond square-based pyramid shaped tip which is pressed into the material with a known force. This leaves a well-defined imprint on the material as shown in **Figure 44**. The hardness is measured from the residual imprint following the **Ec.2**.

$$HV = \frac{Test\ force\ (kgf)}{Surface\ area\ of\ identation\ (mm^2)} = \frac{1}{g_n} * \frac{F}{\frac{d^2}{2*\sin\frac{\alpha}{2}}} \approx 0{,}1819\frac{F}{d^2} \qquad \textbf{(2)}$$

where g_n = 9,80665 m/s^2, *F* is the test force, *d* is the average length of the two diagonal of the imprint and *α* is the angle between opposite faces of the pyramid, see **Figure 44**.
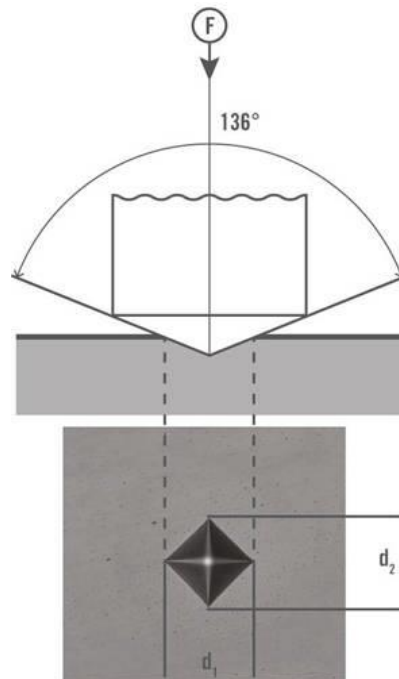
Figure 44. *Scheme of Viker's hardness identation diagonal measurement* (48)*.*

The *H* measurements made in this Bachelor's project are performed with a "DuraScan 10" Microhardness tester (EmcoTest), see **Figure 45**. Equipped with two lenses, one with 10x magnification to see the surface and identify which area is the most suitable for measurement and the other with 50x magnification to be able to observe the imprint detail. In each sample 10 indentations were done at a 5kgf (5HV) of maximum applied load. This load was selected to in order to obtain data without the effect of the defects present in the printed sample and to be able to compare them with the other samples. Test were also performed with a load of 1kgf (1HV) on the 3Y-ZrO$_2$ samples after the LTD as the printed samples could not withstand the 5HV load.

Figure 45. *DuraScan 10 Microhardness tester (EmcoTest)*

The hardness test imprint was also used to measure the indentation fracture toughness (K_{IC}) of the different samples. Indentation toughness measurements methods use the size cracks emanating from the vertices of the Vickers imprints to determine K_{IC}. The lengths of the cracks are in inverse proportion to the toughness of the material. At low loads, Palmqvist cracks are usually formed, the morphology of this cracks is shown in **Figure 46**. To determine the value of the fracture toughness there are several equations that can be used, as a low load was used in this project, the Niihara model has been used, in **Ec. 3** can be seen this equation (49).

$$K_{IC} = 0,0089 * \left(\frac{E}{HV}\right)^{\frac{2}{5}} * \frac{F}{a*l^{0,5}} \; ; \; for \; 0,25 < \frac{l}{a} < 2,5 \tag{3}$$

where *E* is the elastic modulus (GPa), *HV* is the Vickers's hardness (GPa), *F* is the applied load, *c* is the crack length from the centre of the indentation to the crack tip (m), *a* is a half of the indentation diagonal (m) and *l* is the crack length measured from the vertices of the indentation to the crack tip (m).
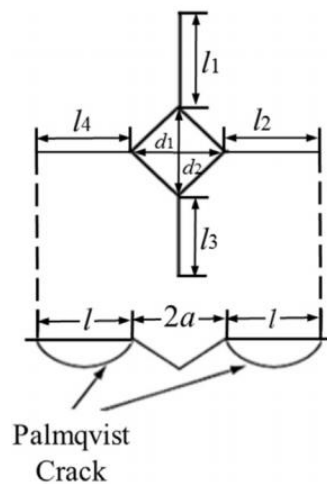
Figure 46. *Palmqvist crack system developed from Vickers indentation* (49).

3.4.2.   Nanoindentation

Nanoindentation can be used to determine local properties at nanometric scale. The main advantages of this technique are that it measures *H* and elastic modulus (*E*) automatically at the same time. Therefore, it is possible to determine the K_{IC}, yield strength (σ_{ys}) and nowadays they are implementing a way to determine the creep behaviour and viscoelastic properties depending on the indenter tip. This technique allows to do an almost full characterization of the elastic and elastoplastic behaviour of the material. This test implies a penetration of 0.2 μm.

The method of this test is similar to the Vickers hardness test. In the **Figure 47** is shown the form of the indentation. The indenter with an increasing normal load *(P)* is applied to the surface, a sensor measures the change in depth *(h)*. At the end, the indenter is unloaded at the same velocity. The obtained data is a load vs indentation depth curve (see **Figure 48**) that provide mechanical data of the material studied.
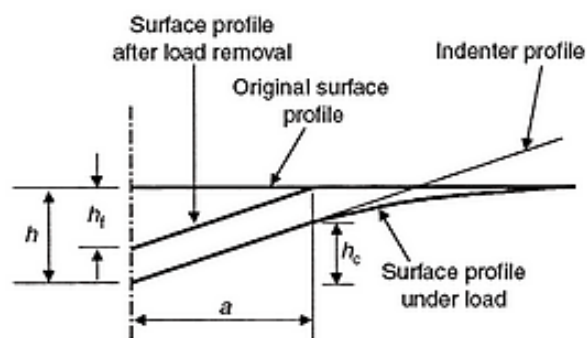
Figure 47. *Diagram of the nanoindentation imprint cycle* (50).

UNIVERSITAT POLITÈCNICA DE CATALUNYA
BARCELONATECH
Escola d'Enginyeria de Barcelona Est
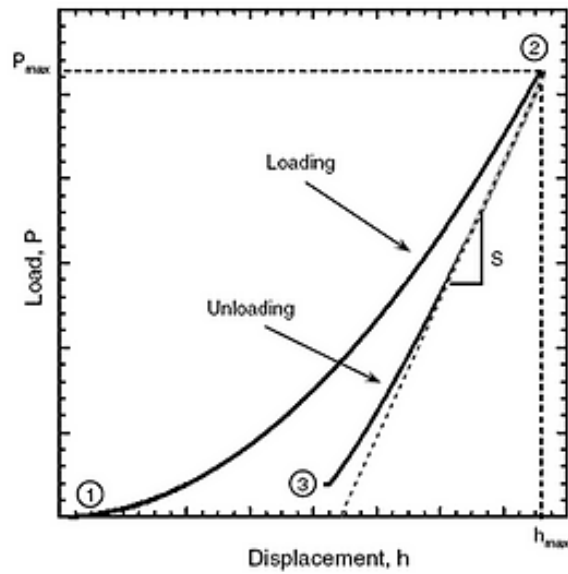
Figure 48. *Graphic result of a nanoindentation test* (50)*.*

In this Bachelor's degree this test was done to obtain a map of *H* and of the *E* of the samples before degradation and after. The machine used was an *iMicro®* (KLA Tencor) nanoindenter, as seen in **Figure 49**. It was done one indentation map in the CIP and LTD samples of 12Ce/3Y-ZrO$_2$, these maps were done with 1600 indents per map on 400 x 400 µm^2 area with a target load of 10 mN and 1.5 µm spacing between indentations.

Figure 49. *iMicro® (KLA) nanoindenter.*

4.   Results and discussions

In this section, the data obtained will be analysed and compared. First, the result of the powder characterization, then the sintered samples characterization and finally the manufacturing techniques will be analysed.

4.1.   Powder characterization

4.1.1.   Particle Size

In order to know if the different powders being used in this Bachelor's degree project are feasible for printing, the maximum particle size has to be studied.

Each material was subjected to a LD study, in the **Figure 50** can be seen the two studies done to 3Y-ZrO_2. This sample shows the biggest change when using the ultrasounds. To better understand this difference the powder was observed by SEM, as is shown in **Figure 51**. By analysing the two figures together, this change can be better understood. The 3Y-ZrO_2 powders from conglomerates which, when mixed with ultrasound, separate into much smaller particles, this causes a bimodal particle size distribution.
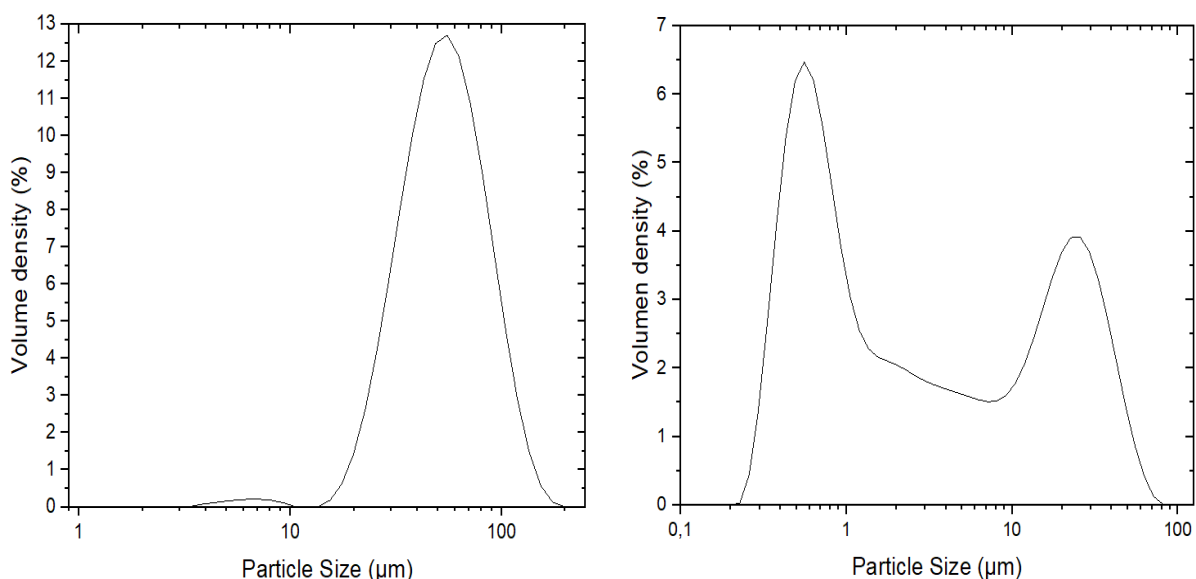
Figure 50. *Size distribution of the 3Y-ZrO_2 powder, (left) mixed with 3500 rpm, (right) ultrasounds.*

UNIVERSITAT POLITÈCNICA DE CATALUNYA
BARCELONA**TECH**
Escola d'Enginyeria de Barcelona Est
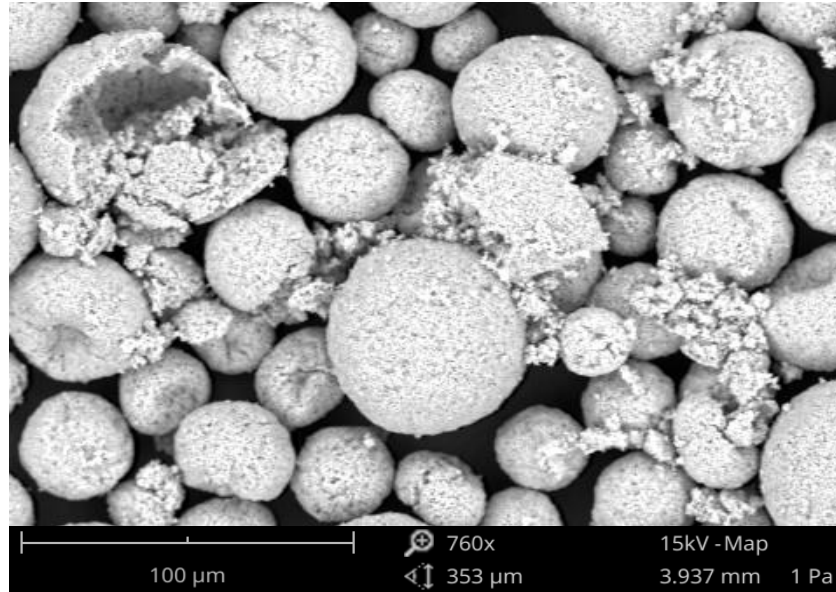
Figure 51. *SEM micrographs of the 3Y-ZrO$_2$ powders.*

The 12Ce-ZrO$_2$ and the composite showed very similar behaviour between them and the particle size distribution was very similar in the two test conditions. The size distribution graphs of these powders are shown in **Figure 52**.
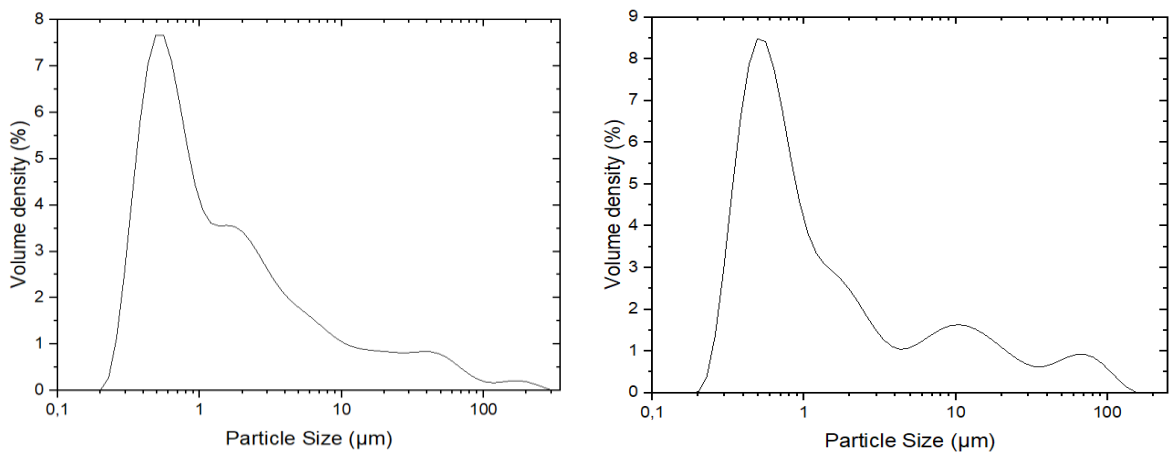
Figure 52. *Size distribution by ultrasounds of 12Ce-ZrO$_2$ (left) and composite (right).*

The powders from these samples were also observed in the SEM to see the powder morphology, as expected these two are very similar since the composite contains a large amount of 12Ce-ZrO$_2$. The two different micrographs are presented in the **Figure 53**. As it has been observed before, these powders have very small particle sizes and the equipment used could not give such a good quality as for the 3Y-ZrO$_2$ image.
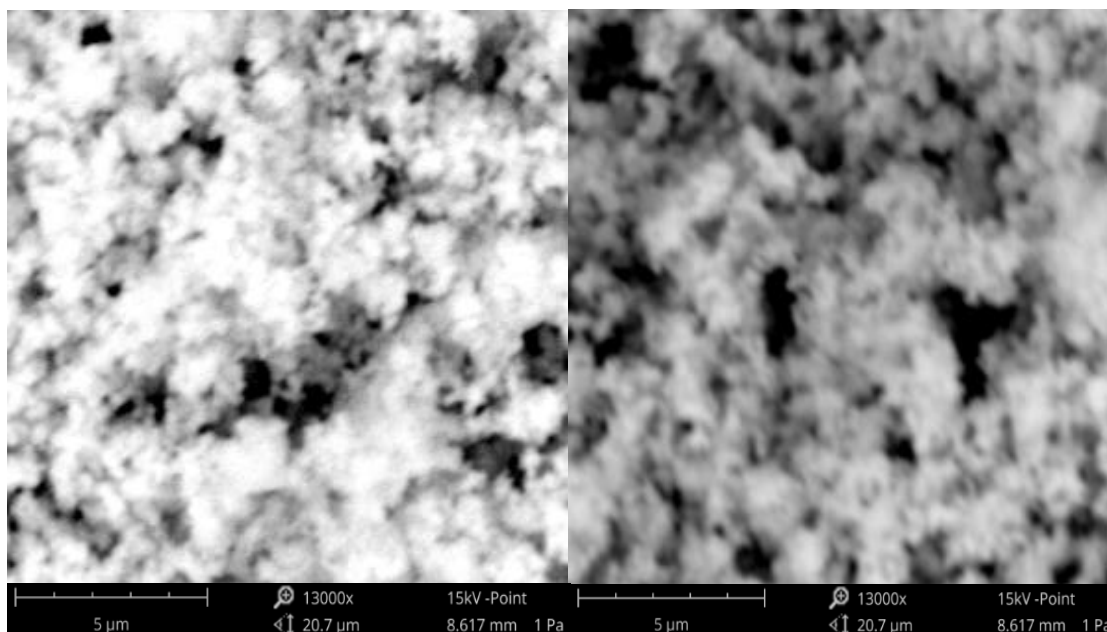
Figure 53. *SEM micrographs of the 12Ce-ZrO$_2$ (left) and the composite (right)*

Table 5 summarizes the maximum particle size found with the LD technique of each of the powders. Analysing the data obtained can be stated that these samples can be used for printing as their maximum particle size does not exceed the size of the nozzle. These values are an approximation that serve as a guide to know if it is possible to print, since the maximum sizes found may not be the real ones, as it is a volume density study.

On the other hand, the results obtained from this test show that the 3 investigated powders have a multimodal particle size distribution. In this sense, the particle size distribution is centered around two or more particle sizes. This will result in samples made with these powders having better mechanical properties, as the combination of particle sizes will help reduce pores in the microstructure and improve the sintering process by increasing particle interface touching.

Table 5. *Maximum particle size of the powders without Ultrasounds.*

Material	Maximum particle size (μm)
3Y-ZrO$_2$	224.95
12Ce-ZrO$_2$	197.99
12Ce/3Y-ZrO$_2$	134.99

4.1.2. *Chemical analysis: EDX*

EDX analysis was carried out to determine the different elements present in the powders that were going to be used. It was important to know the elements present in the powders in order to know if there were any contaminants. **Figure 54** shows the result of the study of $3Y-ZrO_2$ and $12Ce-ZrO_2$. In the two analyses, no foreign elements were found, so that the powders used could be used to make the desired composite. The hafnium (Hf) present in the $3Y-ZrO_2$ powder corresponds to hafnium oxide (HfO_2) which is used to improve the stabilization of the *t*-phase.
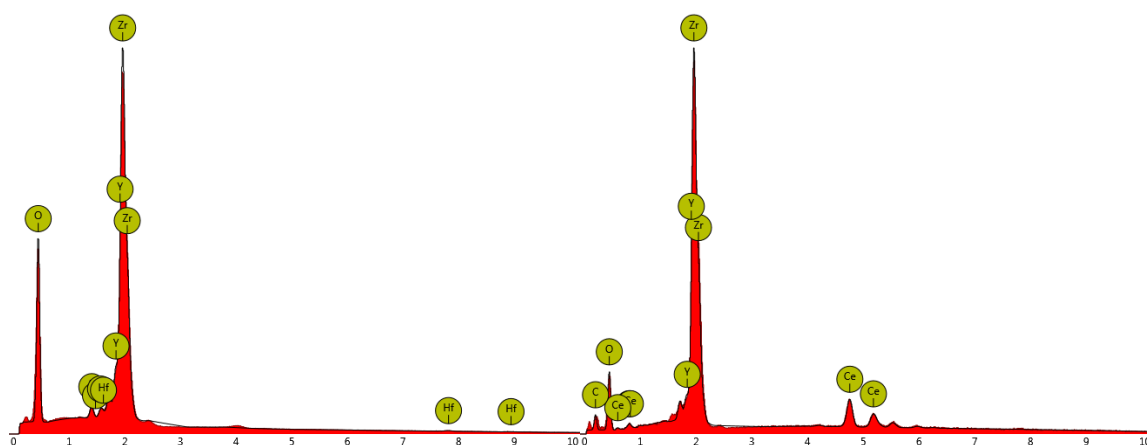
Figure 54. *EDX diagram of $3Y-ZrO_2$ (left) and $12Ce-ZrO_2$ (right).*

The ceramic composite was also analysed with this technique. The result obtained was very similar to the one obtained for the $12Ce-ZrO_2$ but with presence of HfO_2, this analysis is shown in **Figure 55**. But in this case this analysis was done also for verify approximately the amount of 12 Ce and 3Y present in the powder. The powder obtained according to the EDX analysis had a percentage of each stabiliser of 84% CeO_2 and 16% Y_2O_3.
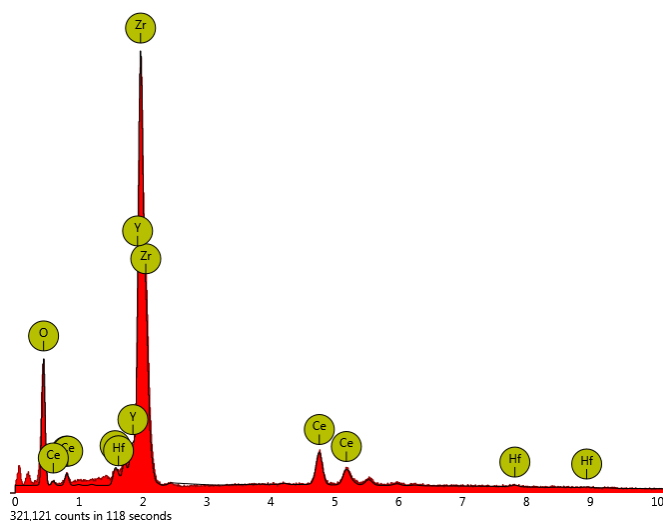
Figure 55. *EDX analysis of the composite.*

UNIVERSITAT POLITÈCNICA DE CATALUNYA
BARCELONA**TECH**
Escola d'Enginyeria de Barcelona Est

49

4.1.3.   X-Ray Diffraction

In order to finish the characterisation of the powders, an XRD test was carried out to determine the crystalline phases present in the raw powders. The results were normalised in order to compare the phases present in each of them. The graphs obtained can be found in **Figure 56**, in this case the results obtained were compared with an XRD study of the ZrO_2 to identify the peaks of the crystalline planes. The reference was found in several articles and with this information was possible to identify the *t*- and *m*-phase peaks in the powders prior to any heat treatment (4)(51). The three powders studied show very few differences in the crystalline phases, there are some variations in the intensity recorded but none of them has a crystalline phase that is not present in the other powders.
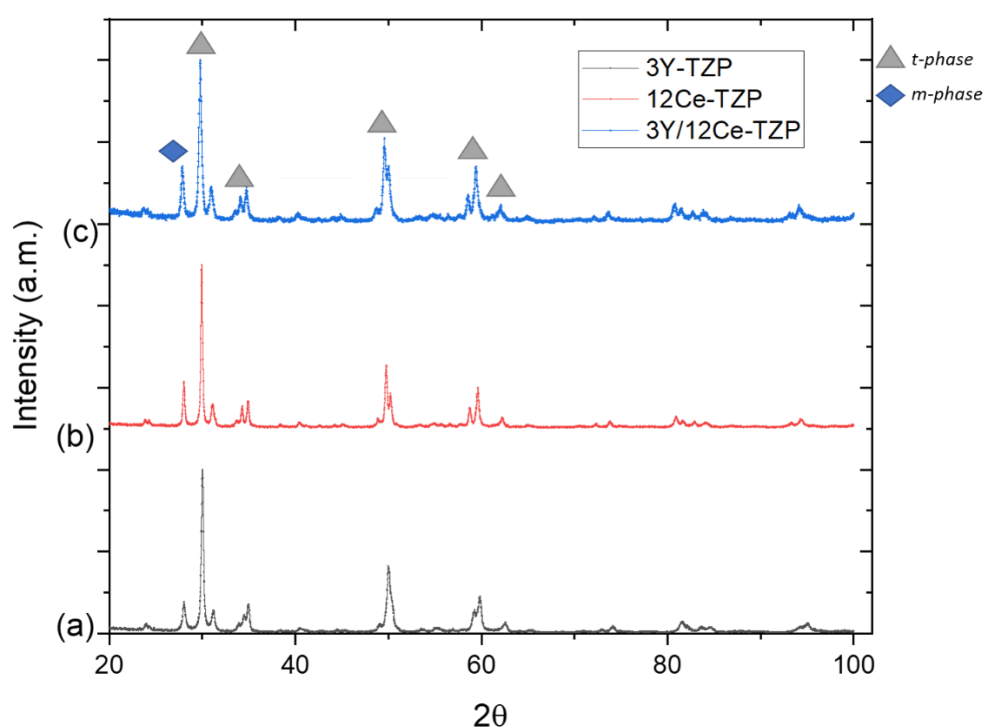
Figure 56. *XRD spectra of the three investigated powders.*

4.2.   Sample characterization

Once the powders were characterized, the samples were made with CIP and 3D printing. The density, hardness, indentation fracture toughness and elastic modulus of the samples were determined with the techniques explained in the experimental methodology. Once this first characterization was done, a sample of each material and each forming method was put in an autoclave to observe how the LTD affected the mechanical properties.

UNIVERSITAT POLITÈCNICA DE CATALUNYA
BARCELONA**TECH**
Escola d'Enginyeria de Barcelona Est

4.2.1. Density

The density was measured to observe if the sample made by CIP had the density close to the theoretical density and to compare this with the density obtained on the printed samples. In addition, the density of the uniaxially pressed machining specimens was also measured.

Table 6 shows the density measurements of the samples together with the theoretical density and the percentage deviation between these two values. It is important to note that the density of the composite is a relative density found using the expression in **Ec.4**.

$$85\% * \rho_{12Ce-ZrO_2} + 15\% * \rho_{3Y-ZrO_2} = 6{,}2075 \frac{g}{cm^3} \tag{4}$$

Table 6. *Density measures of the samples characterized.*

		CIP		3D-Printed		Uniaxial pressing	
	Theoretical density (ρ_t) (g/cm^3)	*Experimental density (ρ_e) (g/cm^3)*	*$\frac{\rho_t}{\rho_e}$ (%)*	*Experimental density (ρ_e) (g/cm^3)*	*$\frac{\rho_t}{\rho_e}$ (%)*	*Experimental density (ρ_e) (g/cm^3)*	*$\frac{\rho_t}{\rho_e}$ (%)*
3Y-ZrO$_2$	6.08	6.067 ± 0,004	99.78 %	5.283 ± 0.014	86.89 %	6.053 ± 0.002	99.56 %
12Ce-ZrO$_2$	6.23	6.237 ± 0,003	99.88 %	5.816 ± 0.052	93.35 %	6.216 ± 0.008	99.77 %
12Ce/3Y-ZrO$_2$	6.21	6.13 ± 0,04	98.71 %	5.756 ± 0.042	92.69 %	6.166 ± 0.004	99.29 %

As can be seen, all the samples made with CIP have a density similar to the theoretical density. This is a good sign as the properties obtained in these samples will be similar to those found in the other studies.

It can also be observed that the samples made by 3D printing have a lower density, this is due to the fact that when 3D printing, many more pores are generated in its microstructure as the body is not completely solid before sintering, as it contains a percentage of Pluronic F-127®. Although the density is lower, the value obtained has been more or less expected and in the cases of the 12Ce-ZrO$_2$ and the composite the density has not dropped below 90 %. In the case of the 3Y-ZrO$_2$ the density may have

been reduced by the particle size. The smaller contact surface between particles and the presence of Pluronic have caused this sample not to densify as much as the other materials studied.

4.2.2. Grain Size

In order to determine the grain size present in the samples studied, it was carried out a thermal etching, at 150 $^\circ$C below the sintering temperature, after this process the samples were observed in the FE-SEM and the grains were counted by means of the LIM to determine the mean value of the grain size, as shown in **Table 7** and the three micrographs taken with this technique are shown in **Figure 57**. **Figure 57b**, shows the microstructure of the composite, this sample have not been successfully etched, so the value of the grain size could not be accurately determined, but it was possible to approximate a value. The obtained grain size are in concordance with this reported in (27).
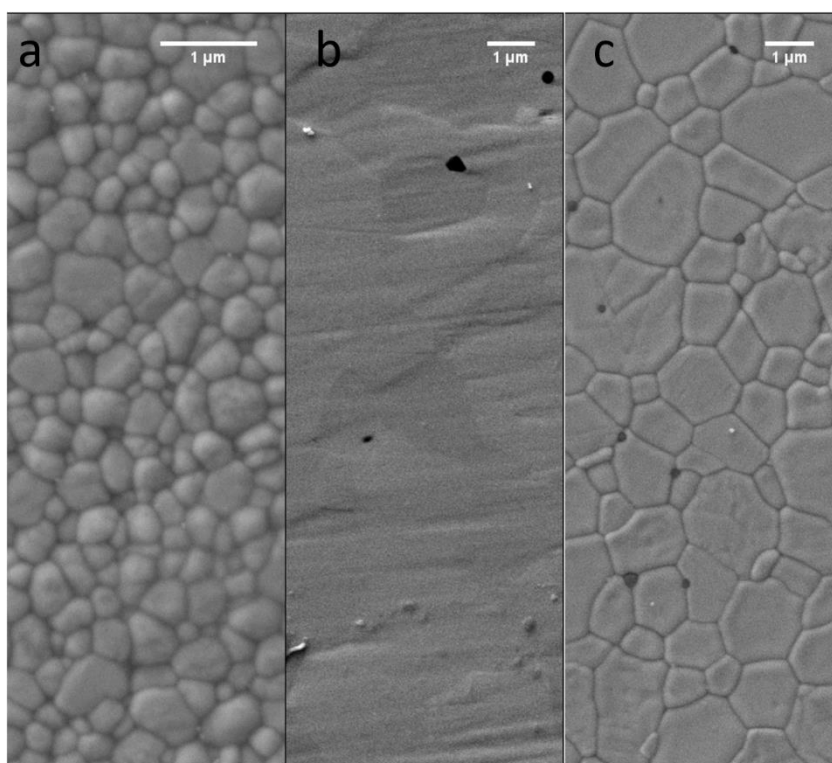
Figure 57. *FE-SEM micrographs of: a) 3Y-ZrO$_2$, b) composite and c) 12Ce-ZrO$_2$.*

Table 7. *Mean value of the grain size.*

	3Y-ZrO$_2$	**Composite**	**12Ce-ZrO$_2$**
Grain Size (μm)	0.31 ± 0.14	1.24 ± 0.62	1.18 ± 0.51

As can be seen, 3Y-ZrO$_2$ has a smaller grain size than 12Ce-ZrO$_2$. The 85/15-ZrO$_2$ composite should have a slightly smaller grain size than the 12Ce-ZrO$_2$ sample, but the data obtained indicate that the grain size is slightly larger. This is due to the sintering process was made at higher temperatures and the grains were able to grow larger in concordance with (27)**.**

While observing the FE-SEM micrographs, the edges of the residual imprints were observed on the 12Ce-ZrO$_2$ sample. **Figure 58** shows two of these cracks and it can be seen how these cracks propagate along the grain boundaries where it needs less energy to propagate.
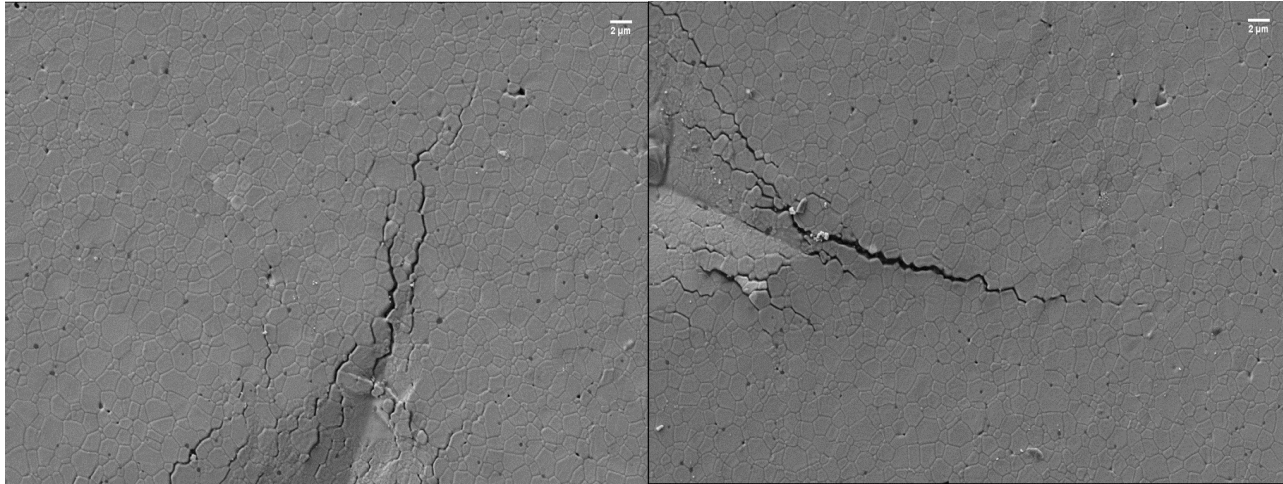
Figure 58. FE-SEM image of the cracks on the imprint indentation tip on the 12Ce-ZrO sample.

4.2.3.　　Hardness and indentation fracture toughness

To determine the hardness and indentation fracture toughness, tests were carried out with a Vickers indenter. The cracks formed from the tips of the indentation were used to determine the fracture toughness of the materials. Therefore, photos were taken of most of the indentations made, the first pictures were taken in the SEM, but due to technical problems the last pictures had to be taken in the OM. It should be noted that in the case of 12Ce-ZrO$_2$ and the composite, these cracks sometimes did not meet the necessary conditions to be evaluated, as shown in **Figure 59b**. The reason for this is that as the material is softer, which implies that the fracture toughness is higher and it is difficult to induce and propagate cracks at the edges of the imprints.
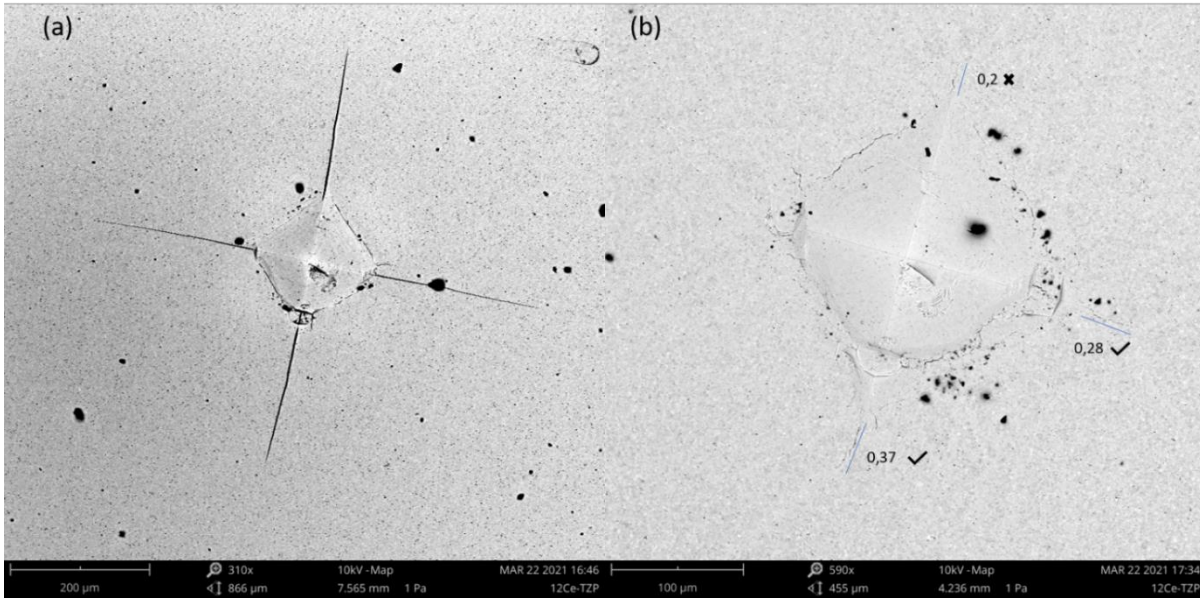
Figure 59. *Indentation observed from SEM, 3Y-ZrO$_2$ (a) and 12Ce-ZrO$_2$ (b) the blue lines mark the distance of propagation and whether they meet the condition.*

This process was done to both CIP and printed samples and in **Figure 60** the behaviour of these properties can be observed according to the material and the method. Moreover, Table **8** summarizes the mean values for both mechanical properties.
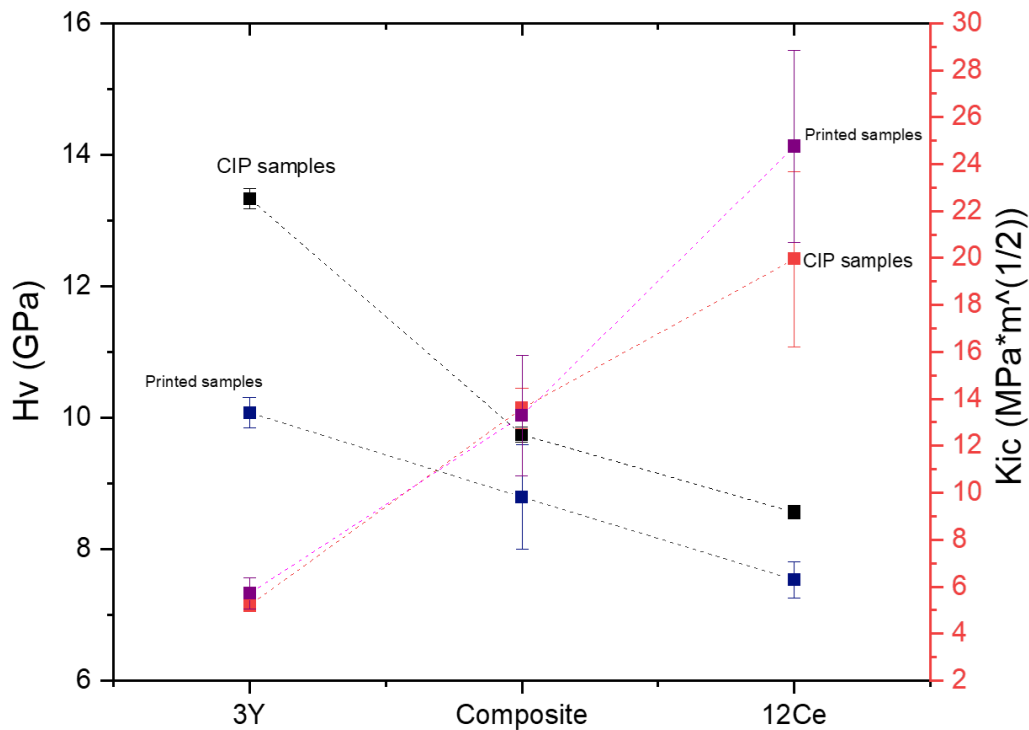
Figure 60. *Hardness and indentation fracture toughness for non-degraded samples.*

UNIVERSITAT POLITÈCNICA DE CATALUNYA
BARCELONATECH
Escola d'Enginyeria de Barcelona Est

Table 8. *Values of hardness and indentation fracture toughness summarized for non-degraded samples*

Hardness (GPa)	CIP	13.33 ± 0.156	9.74 ± 0.12	8.56 ± 0.1
	3D	10.07 ± 0.23	8.79 ± 0.80	7.53 ± 0.27
Fracture toughness (MPa*m$^{1/2}$)	CIP	5.21 ± 0.27	13.59 ± 0.86	19.95 ± 3.73
	3D	5.71 ± 0.65	13.28 ± 2.56	24.76 ± 4.08
	Sample type	**3Y-ZrO$_2$**	**Composite**	**12Ce-ZrO$_2$**

As can be seen, hardness and the indentation fracture toughness are inverse, i.e. if one increases it will result in the reduction of the other. The composite, which is the material for which this work is being done, has a low hardness of almost 10 GPa, together with a higher indentation fracture toughness than the 3Y-ZrO$_2$. On the other hand, the printed samples show a drop in their hardness, which leads to an increase in the indentation fracture toughness.

In the **Figure 61** is shown picture of a residual indentation on 3Y-ZrO$_2$ printed sample, where the pores of the sample can be observed. The 3Y-ZrO$_2$ and the composite shows a similar behaviour in fracture toughness, the CIP samples and the 3D printed ones has similar properties in both materials. In contrast, the 12Ce-ZrO$_2$ samples show a considerable increase in fracture toughness, although in terms of hardness it has a smaller decrease between CIP and 3D printed samples as the composite.
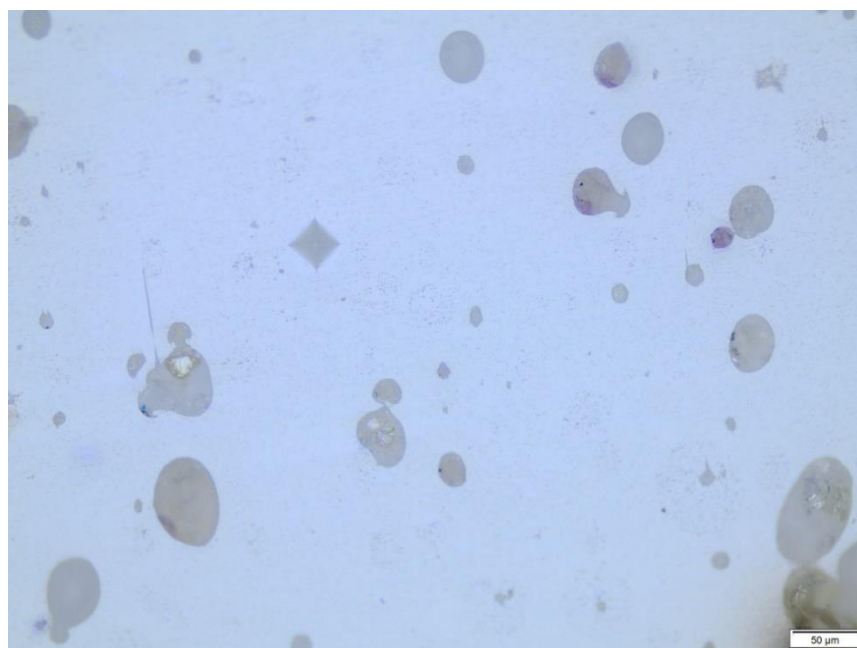
Figure 61. *Picture of the OM showing the surface of the 3Y-ZrO$_2$ printed sample.*

UNIVERSITAT POLITÈCNICA DE CATALUNYA
BARCELONA**TECH**
Escola d'Enginyeria de Barcelona Est

Once the hardness tests were done, a sample of each material and each processing technique was polished again and placed in the autoclave to observe how LTD affected them. In Figure **62** are shown the values of hardness and indentation fracture toughness of the materials after the LTD. Moreover, in the **Table 9** are shown the mean values for both mechanical properties.
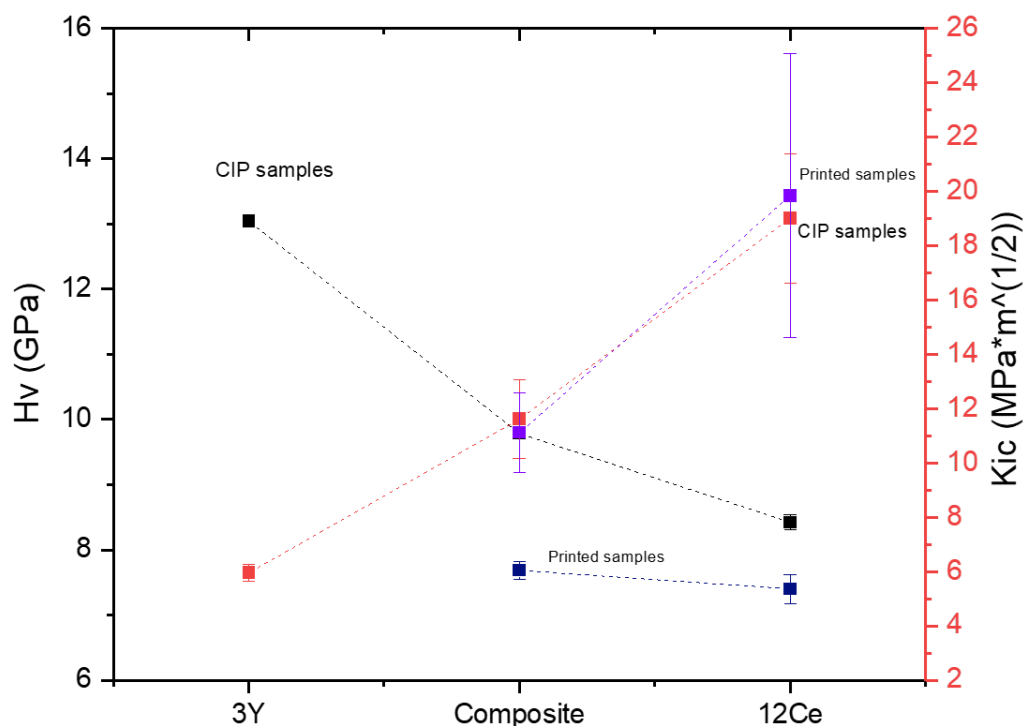
Figure 62. *Hardness and indentation fracture toughness evolution for the degraded samples.*

Table 9. *Summary of hardness and indentation fracture toughness for degraded samples.*

Hardness (GPa)	*CIP*	13.04 ± 0.08	9.78 ± 0.05	8.42 ± 0.12
	3D	-	7.68 ± 0.14	7.39 ± 0.22
Fracture toughness (MPa*m$^{1/2}$)	*CIP*	5.95 ± 0.31	11.62 ± 1.45	19.01 ± 2.38
	3D	-	11.11 ± 1.47	19.83 ± 5.23
	Sample type	**3Y-ZrO$_2$**	**Composite**	**12Ce-ZrO$_2$**

Is important to be noted, that as can be seen in **Figure 63**, when doing the hardness test at 5 Kgf on 3D printed 3Y-ZrO$_2$ samples a decohesion around the indentation is produced, being impossible to determine the indentation fracture toughness. The 3D printed sample shows a

much higher LTD than the other, due to being stabilised by Y_2O_3, which generates a structure with vacancies and due to the high porosity induced during the 3D printing process which allows water vapour to penetrate inside the material.
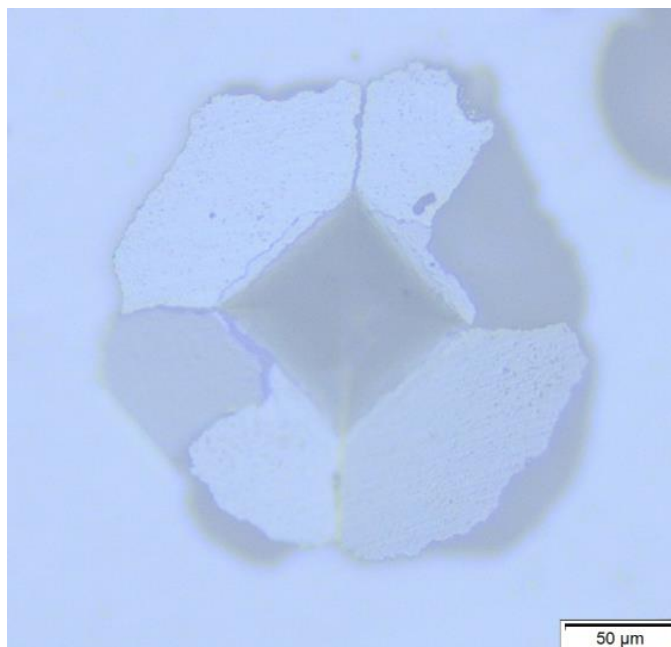
Figure 63. *OM micrograph of a Vickers imprint (5HV) in 3Y-ZrO₂.*

The values of the HV1 test are summarized in **Table 10.**

Table 10. *Values of hardness and indentation fracture toughness for 3Y-ZrO₂ for the LTD samples.*

Hardness (GPa)	*CIP*	13.44 ± 0.17
	3D	10.34 ± 0.67
Fracture toughness (MPa*m$^{1/2}$)	*CIP*	6.35 ± 0.31
	3D	6.07 ± 0.26

The 3Y-ZrO₂ samples produced by traditional processing routes (e.g. CIP) has an increase in indentation fracture toughness, on the other hand, the hardness seems to be reduced. On the rother hand, for the 3D printed samples due to the presence of internal defects, the applied load in order to correctly determine the hardness and indentation fracture toughness should be decreased.

It is necessary to mention, that the 12Ce-ZrO₂ samples have maintained their mechanical integrity after the LTD. In this sense, the 3D printed composite after LTD process shows a reduction in their

mechanical integrity. This phenomenon can be attributed to the presence of imperfections produced during the 3D printing process in the microstructure.

4.2.4.   Nanoindentation

Two samples were studied, the composite CIP sample and the composite CIP sample after degradation in order to observe the hardness and elastic modulus as a function of the resulting microstructure.

Figure 64 is shown the hardness and elastic modulus cartography map from the CIP sample without degradation. As it is evident, the values of hardness obtained at the nanometric length scale are higher than the ones obtained in the Vickers test. This effect is mainly attributed to the Indentation Size Effect. In other words, smaller is stronger.

Figure 65 are represented the maps after the LTD. Analysing the mean hardness values, the sample without LTD presents a mean value of 13.8 ± 1.1 GPa and the sample degraded has a value of 14.8 ± 2.2 GPa. These changes in hardness are not what would be expected for a ZrO_2 sample that has undergone LTD, so these changes are likely to be due to the fact that each sample may vary slightly in its mechanical properties.

In the case of the elastic modulus map, both samples present a similar elastic modulus value of around 243 and 242 GPa for the degraded and non-degraded one, respectively. With this test, apart to obtain the elastic modulus to calculate the indentation fracture toughness, it can also be observed that the composite has a high resistance to LTD, as with the data analysed it does not seem to suffered LTD.
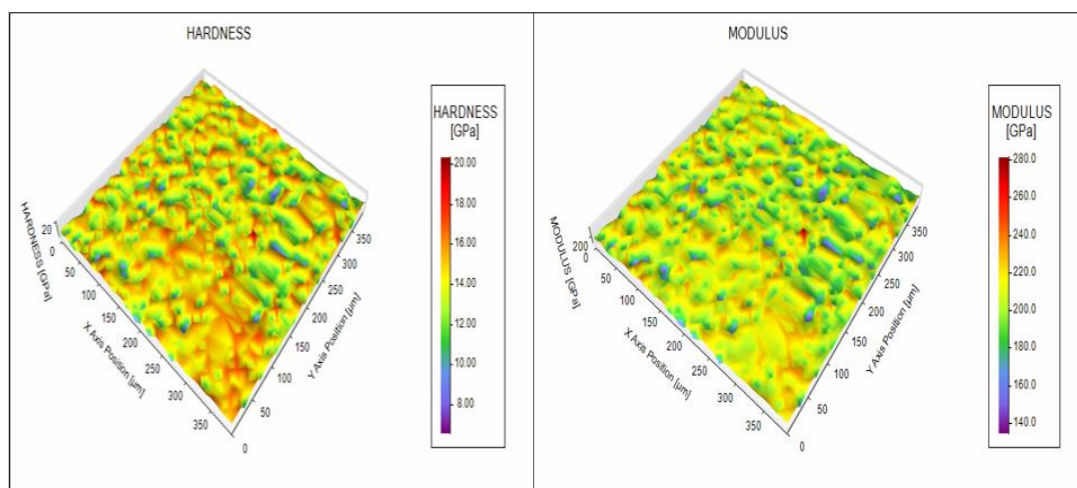
Figure 64. *Hardness (left) and elastic modulus (right) maps before LTD test.*

UNIVERSITAT POLITÈCNICA DE CATALUNYA
BARCELONA**TECH**
UPC   Escola d'Enginyeria de Barcelona Est
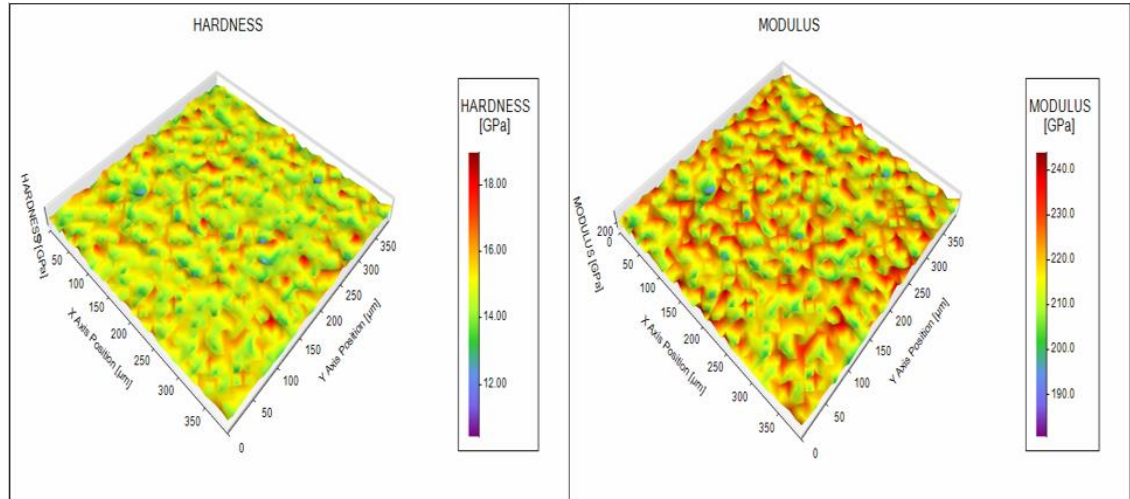
Figure 65. *Hardness (left) and elastic modulus (right) maps after LTD.*

4.2.5. XRD analysis

XRD spectra was carried out to determine the different constitutive phases present in the samples subjected to the LTD test. In this way, the phases present can be found, and it can be determined whether the *t*-phase has undergone a spontaneous change to *m*-phase.

Figure 66 shows the analysis for the LTD samples performed by CIP while in **Figure 67** the analysis for the 3D printed samples after LTD is presented.
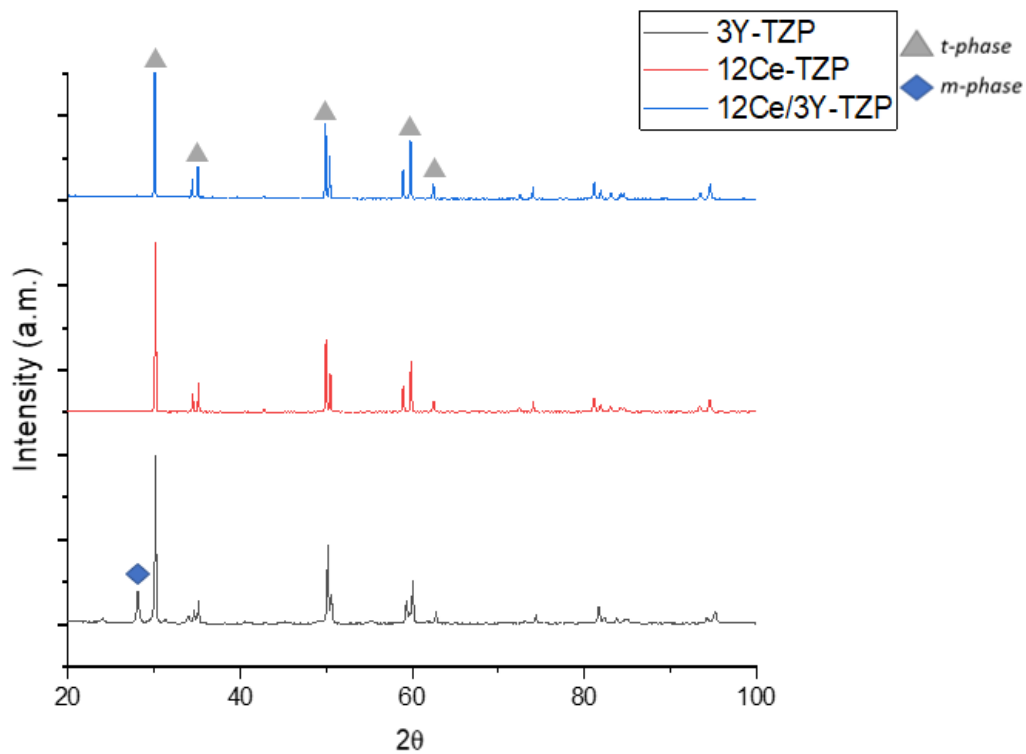
Figure 66. *XDR spectra of the three samples performed by CIP*

Analysing the composite behaviour once the LTD has been made, it can be seen that it has not undergone a phase transformation (*t* → *m)*, which indicates that this material is capable of resisting LTD better than $3Y-ZrO_2$ with an 85% $12Ce-ZrO_2$. Furthermore, comparing **Figures 66** and **67**, the spectra for each investigated material present the same content of *t*-peaks. This highlight that the processing method does not induce any phase transformation.
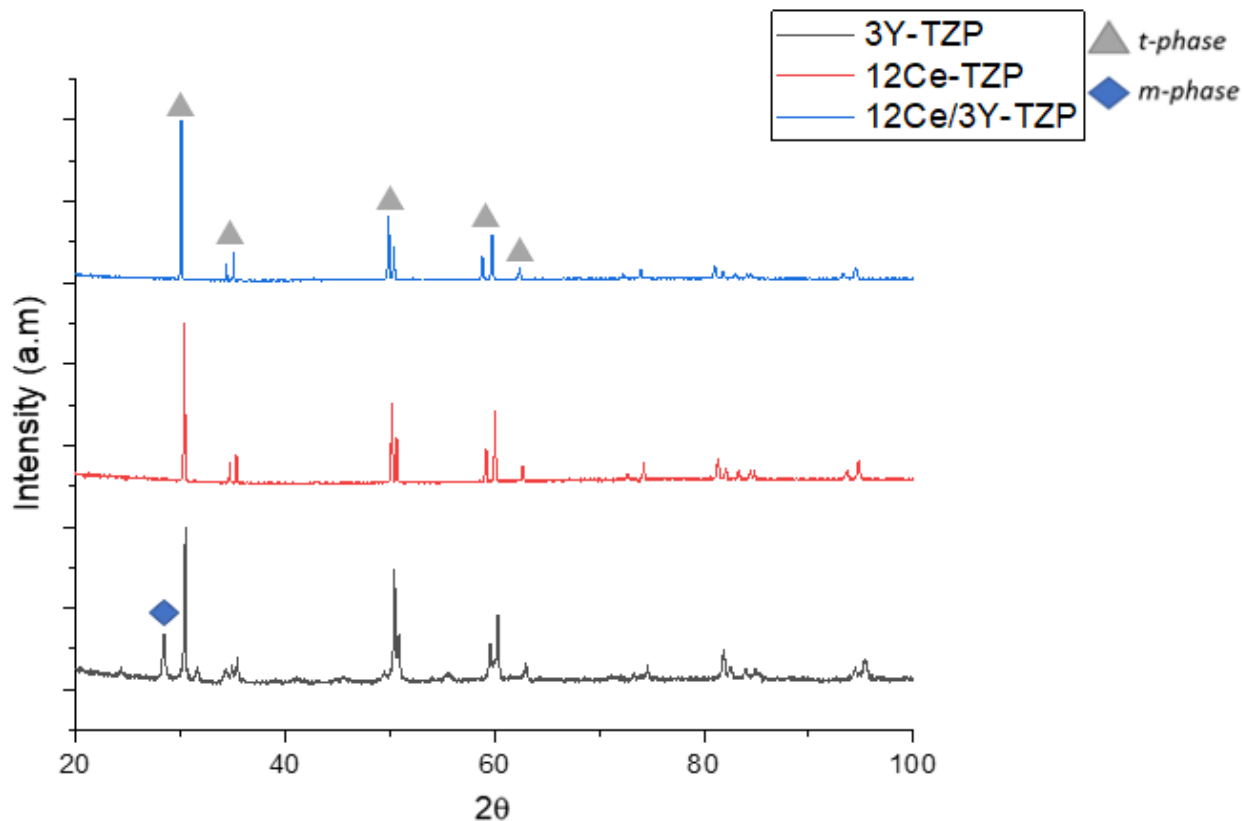
Figure 67. *XDR spectra of the three 3D-printed samples*

4.3. Manufacturing process

4.3.1. Additive manufacture
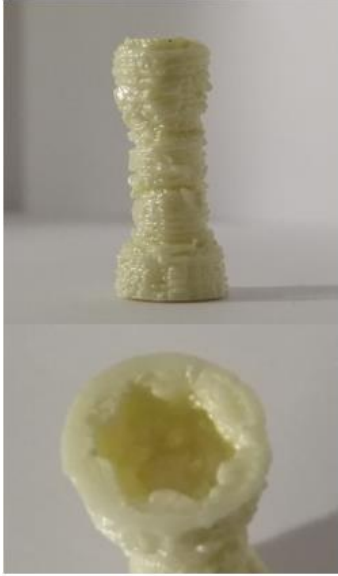
The implant to be printed had a complex and small geometry, so a scaling was carried out to see how each of the materials was printed and whether it would be possible to print a smaller geometry. For this reason, an implant with a height of 35.88 mm was printed. In this case complete implants were printed for the composite and the 12Ce-ZrO_2 materials due to both presents the best properties after LTD.

With these prints it was possible to know approximately the shrinkage that the material suffered when it is sintered, being this value of around 34 %. When trying to print 3Y-ZrO_2 there were problems due to the relative humidity. In order to solve this problem, the specimens were held in a cabinet, for 24 hours. Once it was dry the second printing batch was carried out.

Knowing the shrinkage, to get an implant with the real dimensions, the printed sample should be around 9 mm high. To be able to print with this size, two further reductions were made to see how far

UNIVERSITAT POLITÈCNICA DE CATALUNYA
BARCELONA**TECH**
Escola d'Enginyeria de Barcelona Est
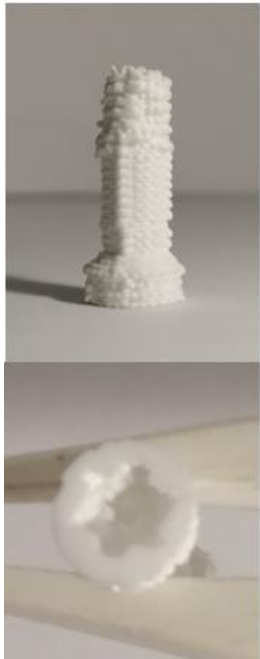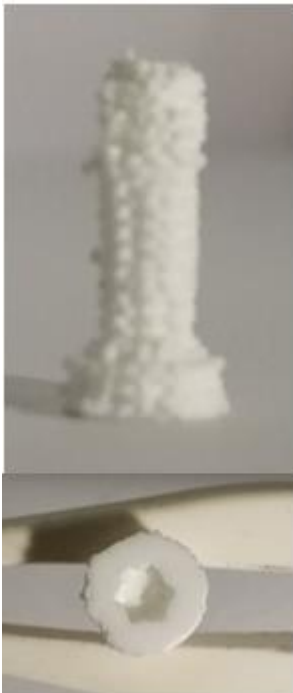
this geometry could be printed with the available printer and if the implant would hold its shape. In the **Table 11** are shown images of each implant after the sintering process.

Table 11. *Images of the different implants printed*

Implant height before sintering/after sintering (mm)	3Y-ZrO$_2$	Composite	12Ce-ZrO$_2$
		Material	
35.88/23.65			

Table 11. *Images of the different implants printed (continuation).*

23.92/16.56			
18.2/11.7			

During the printing process, several drawbacks were encountered when using the DIW technique. Samples with a height if around 36 mm tall were printed without any problems as they followed the desired geometry and the bottom hole was well defined. Although, sometimes due to the duration of

the printing process (≈2 hours) problems were encountered and unwanted defects were found as seen in the 36 mm composite image.

When decreasing the height, another problem was detected, as the "neck" of the implant was smaller, it was suitable to oscillate following the pacing of the nozzle, this was due to the fact that this part had less material and was not as rigid as before. This problem can be observed in the central part of the implants for the composite material as well as for the $12Ce-ZrO_2$ This effect can be reduced by decreasing the 3D printing speed.

For this reason, in order to make the last print, with the lower height as it is much shorter process than the two previous ones, the speed was varied according to the part of the implant that was being printed, paying special attention to the behaviour of each part as it was printed. This allowed the smallest implant to be printed with a shape close to the real geometry. However, in this case the bottom hole was not so well defined as in the other printing cases.

Also, if during the 3D printing impression process exists critical defects, they would make the implant more brittle, as happened in the case of the $12Ce-ZrO_2$. **Figure 68** shows the breakage, this occurs at the neck of the implant as there is less material in this part and the printing process is much faster. Furthermore, by observing the breakage zone it is clearly evident to observe the printing lines in this area. This shows that in that the printability in this area is not good and the adhesion between layers will decrease considerably during the sintering process.

Figure 68. *12Ce-ZrO implant breakage.*

An attempt was made to print smaller implants but the Slic3r program in its simulation already showed that it would not be possible to print, as the infill was too big and each layer had only 3 or 4 passes, making it very poorly defined. On the other hand, possibilities were studied to try to print the implant

with the thread, but it was discarded because when printing these parts could not be supported and would not be as desired and could also damage the printing process of the rest of the implant.

To sum up, all different materials investigated here are capable of printing the implant with greater or lesser precision, but to be able to print it with the real size, a smaller diameter nozzle is required. In order to do that, an exhaustive rheological study should be conducted in order to get the right printability though optimizing the different inks investigated here.

4.3.2.   Machining

To carry out the machining, it was first tried to machine the parts with a thermal process at a lower temperature (900 ⁰C), so that they would not have the final mechanical properties and would be easier to machine. This did not work, as just by fixing the part on the lathe jaws it broke due to the investigated specimens in this case are brittle.

Therefore, the sintered parts were used, first a facing was tried with the CNMG120408, as can be seen in **Figure 69**, the tool could not withstand the properties of the material and the tip brokes. After this failure another tool was tried, this time a complete facing was possible (see **Figure 70**). All tests were first performed on the 12Ce-ZrO_2 parts as this is the softest material. It is important to note that the broken edges are caused by the CIP and not by the machining.

Figure 69. *Tool CNMG120408 with broken tip when attempting to machine*

Figure 70. *Facing in the 12Ce-ZrO$_2$ CIP sample.*

Once the test was done to the CIP samples it is necessary to change the sample geometry in order to be able to clamp the specimen inside the machine. In this sense, the bars were machined in a CNC milling machine due to its rectangular shape. The test was performed with the parameters explained in the section **3.1.1 a**. During this process it was observed how the parts after the tool pass present some black lines in its surface, these footprints are shown in **Figure 71**. It is also important to say that the two machined parts were broken after 4 or 5 passes. This may be due to the imperfections present in the material, due to the samples only were uniaxial pressed. The imperfections acted as a centre of stresses and when the stresses in the part began to increase due to machining, they could propagate more easily. This process was done on the composite and the 12Ce-ZrO$_2$ samples, as they had a lower hardness, the 3Y-ZrO$_2$ sample was not processed due to the high hardness. The surface of the samples after this process was observed in the OM (see **Figure 72**).

Figure 71. *Milling footprints on the 12Ce-ZrO$_2$ sample.*

Figure 72, two parts of the surface of the 12Ce-ZrO$_2$ are shown, in the left image can be seen the lines of the milling process. On the other hand, at the right micrograph the sample without this process can be seen. Observing the two images together can be observed that the surface has not suffered any

UNIVERSITAT POLITÈCNICA DE CATALUNYA
BARCELONATECH
Escola d'Enginyeria de Barcelona Est

significant breakages. Although in the micrograph on the left can be seen how the lines created by the milling tool has piled up the material in some areas as in the upper right part of this image.
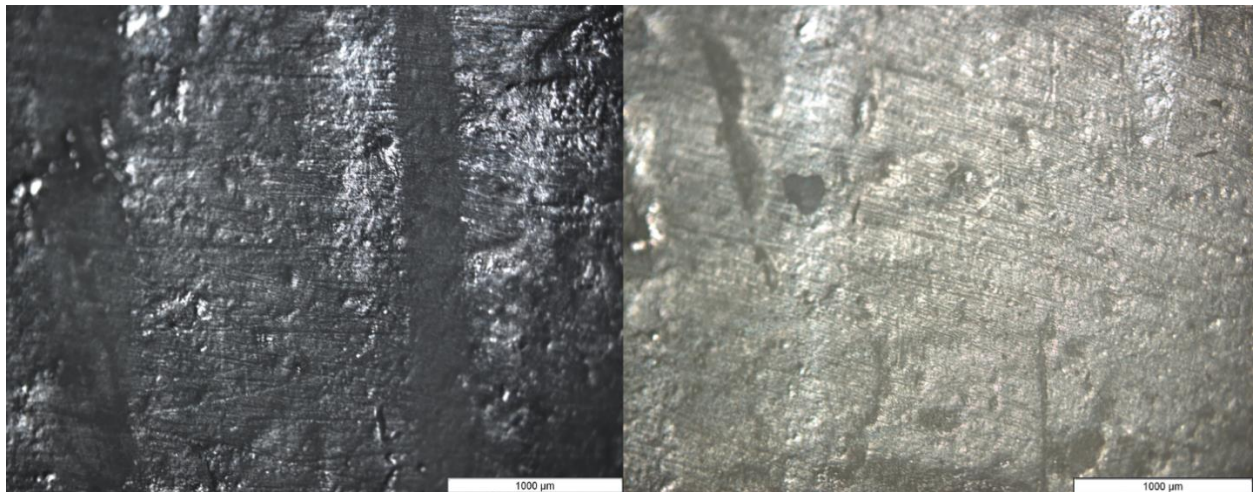
Figure 72. *OM surface micrograph of the 12Ce-ZrO after the milling machine. Left milled surface, right surface without milling process.*

On the other hand, the composite after the milling presented more imprints and seem to has suffered the affect machining more than the 12Ce-ZrO$_2$. This effect can be seen in **Figure 73**, in this micrograph is possible to see how in this case the surface of the material has lost much more of its homogeneity and has become much rougher, tool passes can be detected but because of these it appears that the material has moved and there is less difference in depth between the machined areas and the area through which the tool did not pass. This difference could be caused by the difference of hardness between the two materials, as the composite has a higher hardness and is more resistance to the machining, as well as being more brittle to this process.

Figure 73. *OM surface micrograph of the 12Ce/3Y-ZrO after the milling process*

UNIVERSITAT POLITÈCNICA DE CATALUNYA
BARCELONA**TECH**
Escola d'Enginyeria de Barcelona Est

67

5. Environmental impact analysis

In this section will be analysed the environmental impact related to this Bachelor's project. This analysis will be divided in two parts, in the first part the recyclability and the waste treatment will be evaluated, then in the second part the energy and resources associated to the processing and characterization techniques will be will be analysed.

1. The material used during the process is not very harmful for the environment. During the sample preparation in CIP, care was taken to ensure that there was no loss of material when placing the powders in the mould, and samples that came out wrong or broke were kept so that they could be re-formed into powder, as the part was in green. On the other hand, during the ceramic paste preparation, all the paste tried to be used to avoid the generation of waste, also when cleaning the used tools, i.e. nozzle, syringe, the dirty water and ethanol were stored in buckets to be treated properly.

2. The resources used to characterise and process the materials are mostly water and electricity. Among all the machines used in this Bachelor's project, the process that consumes the most is the furnace, used t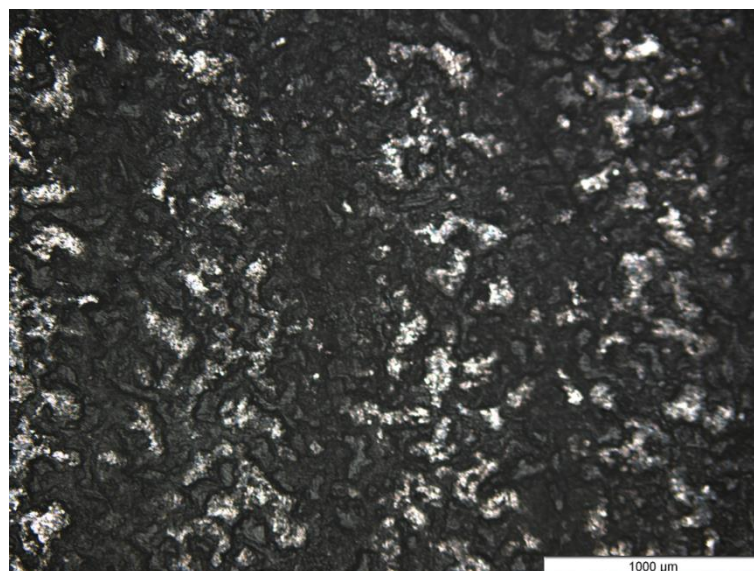o do the thermic treatments, as it is used for long intervals of times and its energy consumption is high. The other techniques, although they also consume electricity to be used, their consumption does not even come close to the consumption of the oven. On the other hand, another critical process is polishing due to the high amount of water used for this process, to reduce the consumption of resources, reusable paper was used to polish. The CNC milling machine could be another critical process due to the use of coolant, but in this case the machine used has a closed circuit that reutilizes the coolant. Other materials used were paper, plastic gloves, among others, these materials were deposited separately in their respective container to be recycled.

Overall, although the energy consumption of the furnace and the water consumption of the polishing machines are high, compared to the energy consumption of other industrial process, the consumption in this project is small. For this reason, it can be said that if the furnace cycles are used efficiently, with as many samples as possible, and if the waste is deposited in the corresponding place to be treated and recycled. This project is not a huge hazard to the environment.

UNIVERSITAT POLITÈCNICA DE CATALUNYA
BARCELONATECH
Escola d'Enginyeria de Barcelona Est

6.   Conclusions and improvements

The characterization of the powders has allowed us to know their size distribution, with this it has been observed that these powders can be used for 3D printing and it has also been studied their particle size distribution, which can be a positive factor to enhance their mechanical properties.

With these powders it has been possible to obtain samples with the mechanical properties expected and registered by other articles, the sample printed with DIW have presented mechanical properties close to those of the samples printed with the same powder. The LTD test has confirmed that the composite does not seem to suffer from LTD since the samples of this material have not suffered changes in their mechanical properties or even phase transformation.

Printing the implants, it has been possible to determine shrinkage when sintering and observe if they could manage to maintain the geometry, and although it has not been possible to print the implant in the real size, it has been proven that with these materials it is possible to print this type of geometry and obtain the desired shape. From the tests carried out it is not possible to determine which option is better, 3D-printing or traditional machining, but it seems that 3D printing is much more promising as there is no risk of braking tools or the material while during the process. During the machining we have seen that without the right tools, machining is very complicated with materials with such high hardness.

6.1.   Improvements

In order to continue this Bachelor's degree and be able to obtain better results, a rheological study of the ceramic ink of the composite could be carried out as well as the feedstock modification in order to be able to use a, nozzle with smaller diameter. This will allow to try to print the implants with the real size and test their resistance in service with wear tests. It would also be interesting to study a way to change the print parameters automatically from the code generated by Slic3r to avoid printing problems and print with more accuracy.

On the other hand, in order to really test whether it is possible to machine these implants using traditional techniques, it is necessary to use tools capable of work with this material without suffering as much war as those used in this project. Another option would be to work with advanced machining techniques such as laser machining.

UNIVERSITAT POLITÈCNICA DE CATALUNYA
BARCELONATECH
Escola d'Enginyeria de Barcelona Est

7. Budget

In this section a financial analysis of this Bachelor's degree project is going to be done.

Table 12. *Summary of the materials used in this Bachelor's project.*

Material

Product	Quantity	Cost/ud.	Cost
3Y-ZrO$_2$	0.5 kg	125 €/kg	62.5 €
12Ce-ZrO$_2$	0.75 kg	125 €/kg	93.75 €
Pluronic F-127	0.1 kg	190 €/kg	19 €
Distilled water	1.5 kg	0.7 €/kg	1.05 €
Ethanol	0,25 L	1,54 €/L	0,39 €
Grinding paper P220	1	0.8 €/un.	0.8 €
Griding paper P1200	1	0.8 €/un.	0,8 €
Cloth MD-Dac	3	53 €/un.	159 €
Cloth MD-Nap	1	75 €/un.	75 €
Diamond suspension 30 μm	0.2 L	90 €/L	18 €
Diamond suspension 6 μm	0.2 L	100 €/L	20 €
Diamond suspension 3 μm	0.2 L	110 €/L	22 €
Colloidal silica suspension	0.1 L	150 €/L	15 €
HSS-Al G-122-003, TiCN, 3mm, 2 flutes. Flatted shank	1	27.14 €/ud.	27.14 €
Total			**514.43 €**

Table 13. *Summary of the equipment used in this Bachelor's project.*

UNIVERSITAT POLITÈCNICA DE CATALUNYA
BARCELONATECH
Escola d'Enginyeria de Barcelona Est

Equipment

Equip	Time of usage	Cost/ud.	Cost
Turbula	96 h	20 €/h	1920 €
Rotavapor	8 h	25 €/h	200 €
Heater	48 h	50 €/h	2400
CIP	10 h	10 €/h	100 €
LD	6 h	60 €/h	360 €
SpeedMixer	0,5 h	5 €/h	2,5 €
3D Printer	14 h	12.4 €/h	173.6 €
Nabathern Furnace	200 h	12.4 €/h	2480 €
Polisher LaboPol-5	15 h	12,4 €/h	186 €
Autoclave	10 h	35 €/h	350 €
OM	12 h	9 €/h	108 €
SEM	4 h	45 €/h	180 €
FE-SEM	1 h	187.50 €/h	187.5
XRD	36 h	56,25 €/h	2025 €
Microindenter	10 h	6 €/h	60 €
Nanoindenter	2 samples	60 €/ud.	120 €
CNC Lathe	1 h	150 €/h	150 €
CNC Milling	2 h	150 €/h	300 €
Total	11302.6 €		

UNIVERSITAT POLITÈCNICA DE CATALUNYA
BARCELONATECH
Escola d'Enginyeria de Barcelona Est

Table 14. *Summary of the personal cost in this Bachelor's project*

Personal costs

Concept	Quantity	Cost/ud.	Cost
Junior Engineer	450 h	25 €/h	11250 €
Senior Engineer	120 h	40 €/h	4800 €
Lab technician	15 h	30 €/h	450 €
Total		16.500 €	

Table 15. *Total cost of the Bachelor's project*

Total cost of the project

Total cost associated with materials	514.43 €
Total cost associated with equipment	11302.6 €
Total cost associated with personal	16.500 €
Total	**28317.03 €**
IVA (21%)	5946.57 €
Total + IVA	**34263.61 €**

8. Bibliography

1. HEUER, A.H. Transformation Toughening in ZrO2-Containing Ceramics. A: *Journal of the American Ceramic Society*. 1987, Vol. 70, núm. 10, p. 689-698.

2. R. T. P. R.C. Garvie. R.H. Hannik. «Ceramic Steel? © 1975 Nature Publishing Group». A: *Nature*. 1975, Vol. 258.

3. Spies, B.C. et al. Reliability and aging behavior of three different zirconia grades used for monolithic four-unit fixed dental prostheses. A: *Dental Materials* [en línia]. The Academy of Dental Materials, 2020, Vol. 36, núm. 11, p. e329-e339. ISSN 01095641. DOI 10.1016/j.dental.2020.08.002. Disponible a: https://doi.org/10.1016/j.dental.2020.08.002.

4. Hwang, K.J. et al. Investigation on the phase stability of yttria-stabilized zirconia electrolytes for high-temperature electrochemical application. A: *Ceramics International* [en línia]. Elsevier Ltd and Techna Group S.r.l., 2019, Vol. 45, núm. 7, p. 9462-9467. ISSN 02728842. DOI 10.1016/j.ceramint.2018.09.026. Disponible a: https://doi.org/10.1016/j.ceramint.2018.09.026.

5. Zucuni, C.P. et al. Grinding the intaglio surface of yttria partially- and fully-stabilized zirconia polycrystals restorations: Effect on their fatigue behavior. A: *Journal of the Mechanical Behavior of Biomedical Materials* [en línia]. Elsevier Ltd, 2020, Vol. 109, núm. April, p. 103800. ISSN 18780180. DOI 10.1016/j.jmbbm.2020.103800. Disponible a: https://doi.org/10.1016/j.jmbbm.2020.103800.

6. Han, Y. i Zhu, J. Surface science studies on the zirconia-based model catalysts. A: *Topics in Catalysis*. 2013, Vol. 56, núm. 15-17, p. 1525-1541. ISSN 10225528. DOI 10.1007/s11244-013-0156-5.

7. Norberg, S.T. et al. Local structure and ionic conductivity in the Zr2Y 2O7-Y3NbO7 system. A: *Journal of Physics Condensed Matter*. 2009, Vol. 21, núm. 21. ISSN 09538984. DOI 10.1088/0953-8984/21/21/215401.

8. Nisticò, R. Zirconium oxide and the crystallinity hallows. A: *Journal of the Australian Ceramic Society*. Journal of the Australian Ceramic Society, 2020, Vol. 1. ISSN 25101579. DOI 10.1007/s41779-020-00529-2.

9. Li, P., Chen, I. -W i Penner-Hahn, J.E. Effect of Dopants on Zirconia Stabilization—An X-ray Absorption Study: III, Charge-Compensating Dopants. A: *Journal of the American Ceramic Society*. 1994, Vol. 77, núm. 5, p. 1289-1295. ISSN 15512916. DOI 10.1111/j.1151-2916.1994.tb05404.x.

10. *DoITPoMS - TLP Library Fuel Cells - • Electrolyte* [en línia]. Disponible a: http://www.doitpoms.ac.uk/tlplib/fuel-cells/sofc_electrolyte.php?printable=1.

11. Li, P., Chen, I. -W i Penner-Hahn, J.E. Effect of Dopants on Zirconia Stabilization—An X-ray Absorption Study: II, Tetravalent Dopants. A: *Journal of the American Ceramic Society*. 1994, Vol. 77, núm. 5, p. 1281-1288. ISSN 15512916. DOI 10.1111/j.1151-2916.1994.tb05403.x.

12. Lughi, V. i Sergo, V. Low temperature degradation -aging- of zirconia: A critical review of the relevant aspects in dentistry. A: *Dental Materials* [en línia]. The Academy of Dental Materials, 2010, Vol. 26, núm. 8, p. 807-820. ISSN 01095641. DOI 10.1016/j.dental.2010.04.006. Disponible a:

http://dx.doi.org/10.1016/j.dental.2010.04.006.

13. Gautam, C. et al. Zirconia based dental ceramics: structure, mechanical properties, biocompatibility and applications. A: *Dalton Transactions*. Royal Society of Chemistry, 2016, Vol. 45, núm. 48, p. 19194-19215. ISSN 14779234. DOI 10.1039/c6dt03484e.

14. Denry, I. i Kelly, J.R. State of the art of zirconia for dental applications. A: *Dental Materials*. 2008, Vol. 24, núm. 3, p. 299-307. ISSN 01095641. DOI 10.1016/j.dental.2007.05.007.

15. Kelly, J.R. i Denry, I. Stabilized zirconia as a structural ceramic: An overview. A: *Dental Materials*. 2008, Vol. 24, núm. 3, p. 289-298. ISSN 01095641. DOI 10.1016/j.dental.2007.05.005.

16. Brook, R. J. Robert, W.C. Concise encyclopedia of advanced ceramic materials. A: *Advanced Materials*. 1992, p. 494-497.

17. Yan, W.Y., Reisner, G. i Fischer, F.D. Micromechanical study on the morphology of martensite in constrained zirconia. A: *Acta Materialia*. 1997, Vol. 45, núm. 5, p. 1969-1976. ISSN 13596454. DOI 10.1016/S1359-6454(96)00320-5.

18. Žmak, I. et al. Hardness and indentation fracture toughness of slip cast alumina and alumina-zirconia ceramics. A: *Materials*. 2020, Vol. 13, núm. 1, p. 1-17. ISSN 19961944. DOI 10.3390/ma13010122.

19. Deville, S., Guénin, G. i Chevalier, J. Martensitic transformation in zirconia part II. Martensite growth. A: *Acta Materialia*. 2004, Vol. 52, núm. 19, p. 5709-5721. ISSN 13596454. DOI 10.1016/j.actamat.2004.08.036.

20. Chevalier, J. et al. The tetragonal-monoclinic transformation in zirconia: Lessons learned and future trends. A: *Journal of the American Ceramic Society*. 2009, Vol. 92, núm. 9, p. 1901-1920. ISSN 00027820. DOI 10.1111/j.1551-2916.2009.03278.x.

21. Borrell, A. et al. Influence of relative humidity and low temperature hydrothermal degradation on fretting wear of Y-TZP dental ceramics. A: *Wear* [en línia]. Elsevier B.V., 2019, Vol. 428-429, núm. January, p. 1-9. ISSN 00431648. DOI 10.1016/j.wear.2019.01.121. Disponible a: https://doi.org/10.1016/j.wear.2019.01.121.

22. Cattani-Lorente, M. et al. Low temperature degradation of a Y-TZP dental ceramic. A: *Acta Biomaterialia* [en línia]. Acta Materialia Inc., 2011, Vol. 7, núm. 2, p. 858-865. ISSN 17427061. DOI 10.1016/j.actbio.2010.09.020. Disponible a: http://dx.doi.org/10.1016/j.actbio.2010.09.020.

23. De Araújo-Júnior, E.N.S. et al. Hydrothermal degradation methods affect the properties and phase transformation depth of translucent zirconia. A: *Journal of the Mechanical Behavior of Biomedical Materials*. 2020, Vol. 112, núm. August. ISSN 18780180. DOI 10.1016/j.jmbbm.2020.104021.

24. Jiménez-Piqué, E. et al. Focused ion beam tomography of zirconia degraded under hydrothermal conditions. A: *Journal of the European Ceramic Society*. 2012, Vol. 32, núm. 10, p. 2129-2136. ISSN 09552219. DOI 10.1016/j.jeurceramsoc.2012.02.011.

25. Chevalier, J., Gremillard, L. i Deville, S. Low-temperature degradation of zirconia and implications for biomedical implants. A: *Annual Review of Materials Research*. 2007, Vol. 37, p. 1-32. ISSN 15317331.

UNIVERSITAT POLITÈCNICA DE CATALUNYA
BARCELONATECH
UPC Escola d'Enginyeria de Barcelona Est

DOI 10.1146/annurev.matsci.37.052506.084250.

26. Liens, A. et al. Phase transformation induces plasticity with negligible damage in ceria-stabilized zirconia-based ceramics. A: *Acta Materialia* [en línia]. Elsevier Ltd, 2020, Vol. 183, p. 261-273. ISSN 13596454. DOI 10.1016/j.actamat.2019.10.046. Disponible a: https://doi.org/10.1016/j.actamat.2019.10.046.

27. Turon-Vinas, M. et al. Mechanical properties of 12Ce-ZrO2/3Y-ZrO2 composites. A: *Ceramics International*. 2015, Vol. 41, núm. 10, p. 14988-14997. ISSN 02728842. DOI 10.1016/j.ceramint.2015.08.044.

28. H. Nielsen, R. i Gerhard, W. Zirconium and Zirconium compounds. A: *Kirk-Othmer Encyclopedia of Chemical Technology*. 2005, núm. 6.

29. Panagiotopoulos, E.C. et al. Early failure of a zirconia femoral head prosthesis: Fracture or fatigue? A: *Clinical Biomechanics*. 2007, Vol. 22, núm. 7, p. 856-860. ISSN 02680033. DOI 10.1016/j.clinbiomech.2007.04.007.

30. Nogiwa-Valdez, A.A., Rainforth, W.M. i Stewart, T.D. Wear and degradation on retrieved zirconia femoral heads. A: *Journal of the Mechanical Behavior of Biomedical Materials* [en línia]. Elsevier, 2014, Vol. 31, p. 145-151. ISSN 17516161. DOI 10.1016/j.jmbbm.2013.09.019. Disponible a: http://dx.doi.org/10.1016/j.jmbbm.2013.09.019.

31. Chevalier, J. What future for zirconia as a biomaterial? A: *Biomaterials*. 2006, Vol. 27, núm. 4, p. 535-543. ISSN 01429612. DOI 10.1016/j.biomaterials.2005.07.034.

32. Monzavi, M. et al. Microstructural analyses of artificial ageing in 5 commercially and non-commercially available Zirconia dental implants. A: *Journal of the European Ceramic Society* [en línia]. Elsevier, 2020, Vol. 40, núm. 10, p. 3642-3655. ISSN 1873619X. DOI 10.1016/j.jeurceramsoc.2020.03.050. Disponible a: https://doi.org/10.1016/j.jeurceramsoc.2020.03.050.

33. Höland, W. i Beall, G.H. *Glass-Ceramics*. 2013. ISBN 9780123854704. DOI 10.1016/B978-0-12-385469-8.00021-6.

34. Engineering articles. Engineering Articles. A: *Machining Operation and Types of Machining Tools* [en línia]. 2021. [Consulta: 14 abril 2021]. Disponible a: https://www.engineeringarticles.org/machining-operation-and-types-of-machining-tools/#:~:text=Machining operations are classified into,care of each machining operation.

35. EFunda. Machinig Introduction. A: *Machining: An introduction* [en línia]. [Consulta: 14 abril 2021]. Disponible a: https://www.efunda.com/processes/machining/machin_intro.cfm.

36. Bharathi, V. et al. Materials Today : Proceedings A review on the challenges in machining of ceramics. A: *Materials Today: Proceedings* [en línia]. Elsevier Ltd, 2021, núm. xxxx. ISSN 2214-7853. DOI 10.1016/j.matpr.2021.03.019. Disponible a: https://doi.org/10.1016/j.matpr.2021.03.019.

37. Mehta, K.M., Kumar Pandey, S. i Shaikh, V.A. Unconventional Machining of ceramic matrix Composites – A review. A: *Materials Today: Proceedings* [en línia]. Elsevier Ltd., 2021, núm. xxxx. ISSN 22147853. DOI 10.1016/j.matpr.2021.01.961. Disponible a:

https://doi.org/10.1016/j.matpr.2021.01.961.

38. Atanasov, P.A., Eugenieva, E.D. i Nedialkov, N.N. Laser drilling of silicon nitride and alumina ceramics: A numerical and experimental study. A: *Journal of Applied Physics*. 2001, Vol. 89, núm. 4, p. 2013-2016. ISSN 00218979. DOI 10.1063/1.1334367.

39. Peng, E., Zhang, D. i Ding, J. Ceramic Robocasting: Recent Achievements, Potential, and Future Developments. A: *Advanced Materials*. 2018, Vol. 30, núm. 47, p. 1-14. ISSN 15214095. DOI 10.1002/adma.201802404.

40. Rodrigues, I. et al. Development of free binder zirconia-based pastes for the production of dental pieces by robocasting. A: *Journal of Manufacturing Processes* [en línia]. Elsevier, 2020, Vol. 57, núm. June, p. 1-9. ISSN 15266125. DOI 10.1016/j.jmapro.2020.06.015. Disponible a: https://doi.org/10.1016/j.jmapro.2020.06.015.

41. Osman, R.B. et al. 3D-printing zirconia implants; a dream or a reality? An in-vitro study evaluating the dimensional accuracy, surface topography and mechanical properties of printed zirconia implant and discs. A: *Journal of the Mechanical Behavior of Biomedical Materials* [en línia]. Elsevier Ltd, 2017, Vol. 75, núm. August, p. 521-528. ISSN 18780180. DOI 10.1016/j.jmbbm.2017.08.018. Disponible a: https://doi.org/10.1016/j.jmbbm.2017.08.018.

42. Lim, H.B. et al. Green and hard machining characteristics of zirconia-alumina composites for dental implant. A: *Journal of the Korean Ceramic Society*. 2011, Vol. 48, núm. 2, p. 152-159. ISSN 12297801. DOI 10.4191/KCERS.2011.48.2.152.

43. Nakahira, A. et al. Fabrication and evaluation of high performance 12Ce-ZrO2/3Y- ZrO2 composites for an implant. A: *Journal of the Ceramic Society of Japan*. 2006, Vol. 114, núm. 1335, p. 1076-1080. ISSN 13486535. DOI 10.2109/jcersj.114.1076.

44. Malvern-Panalytical. *Laser Diffraction Particle Size Analysis | Malvern Panalytical* [en línia]. 2020. 2020. Disponible a: https://www.malvernpanalytical.com/en/products/technology/light-scattering/laser-diffraction.

45. Inkson, B.J. *Scanning Electron Microscopy (SEM) and Transmission Electron Microscopy (TEM) for Materials Characterization* [en línia]. Elsevier Ltd, 2016. ISBN 9780081000571. DOI 10.1016/B978-0-08-100040-3.00002-X. Disponible a: http://dx.doi.org/10.1016/B978-0-08-100040-3.00002-X.

46. ASTM E112. Standard Test Methods for Determining Average Grain Size E112-10. A: *Astm E112-10*. 2010, Vol. 96, núm. 2004, p. 1-27. DOI 10.1520/E0112-10.Copyright.

47. Ibañez, P. Grain Size Astm E112. A: .

48. *Vickers test procedure – Hardness Know-How* [en línia]. Disponible a: https://www.emcotest.com/en/the-world-of-hardness-testing/hardness-know-how/theory-of-hardness-testing/vickers/vickers-test-procedure/.

49. Ćorić, D., Majić Renjo, M. i Ćurković, L. Vickers indentation fracture toughness of Y-TZP dental ceramics. A: *International Journal of Refractory Metals and Hard Materials*. 2017, Vol. 64, p. 14-19. ISSN 22133917. DOI 10.1016/j.ijrmhm.2016.12.016.

50. *Nanoindentation Testing Services_ Mechaction_ Fast Turnaround* [en línia]. Disponible a: https://www.mechaction.com/nanoindentation.

51. Zang, S. et al. Influence of additives on the purity of tetragonal phase and grain size of ceria-stabilized tetragonal zirconia polycrystals (Ce-TZP). A: *Ceramics International* [en línia]. Elsevier Ltd and Techna Group S.r.l., 2019, Vol. 45, núm. 1, p. 394-400. ISSN 02728842. DOI 10.1016/j.ceramint.2018.09.179. Disponible a: https://doi.org/10.1016/j.ceramint.2018.09.179.

9. Annexe

9.1. Annexe A: Software

9.1.1.   Annex A1 Slic3er

Available: http://slic3r.org/. visited 25/02/2021

Slic3r is a software that converts a 3D model into a G-code, this code is used to give printing instructions for a 3D printer. It transforms the 3D model into layers, generates the toolpath to fill these layers and calculate the amount of material needed to do the printing process. With this program the main printing parameters can be modified and is needed to change some parameters to adjust the code to the printer that is going to be used for printing.

In the next part the parameters that were needed to be changed during this bachelor's project are briefly explained:

The first parameter that must be modified is the *Printing Settings.*

- *Layer and perimeters:*

In this tab the layer height, the vertical and horizontal shells and the quality of the perimeters can be modified, in the **Figure A.1** the layer and perimeters parameters are shown.
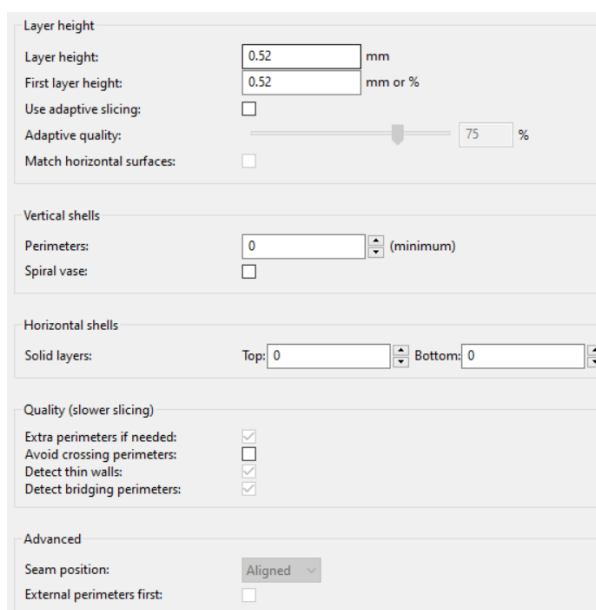
Figure A.1: Layer and perimeters parameters

UNIVERSITAT POLITÈCNICA DE CATALUNYA
BARCELONA**TECH**
Escola d'Enginyeria de Barcelona Est

- *Infill*

In this section can be modified the fill density, the fill pattern among other parameters, as shown in **Figure A.2.**

Figure A.2: Infill parameters

- *Speed*

In this tab is possible to modify the speed for printing moves and for non-printing moves, the parameters of the printer used are shown in **Figure A.3.**

Figure A.3: Speed parameters

- *Skirt and brim*

In this section can be modified the number of loops that make the printer before starting the process, in this Bachelor's project degree it was selected 2 loops.

Secondly the *Printer Settings* have to be modified.

- *General*

In this tab the size and the coordinates of the printer can be modified, the parameters of the printer used are shown in **Figure A.4.**
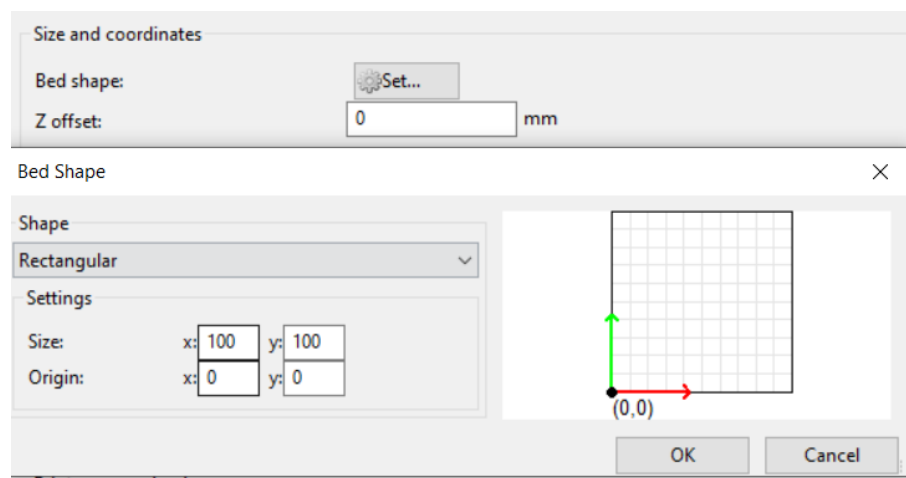

Figure A.4: Size of the bed and print center.

- *Extruder*

In this section the diameter of the nozzle has to be inputted, as shown in **Figure A.5**.
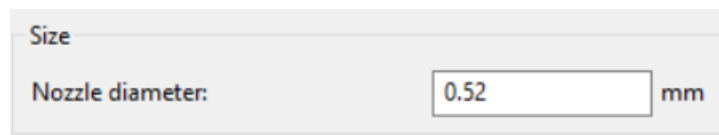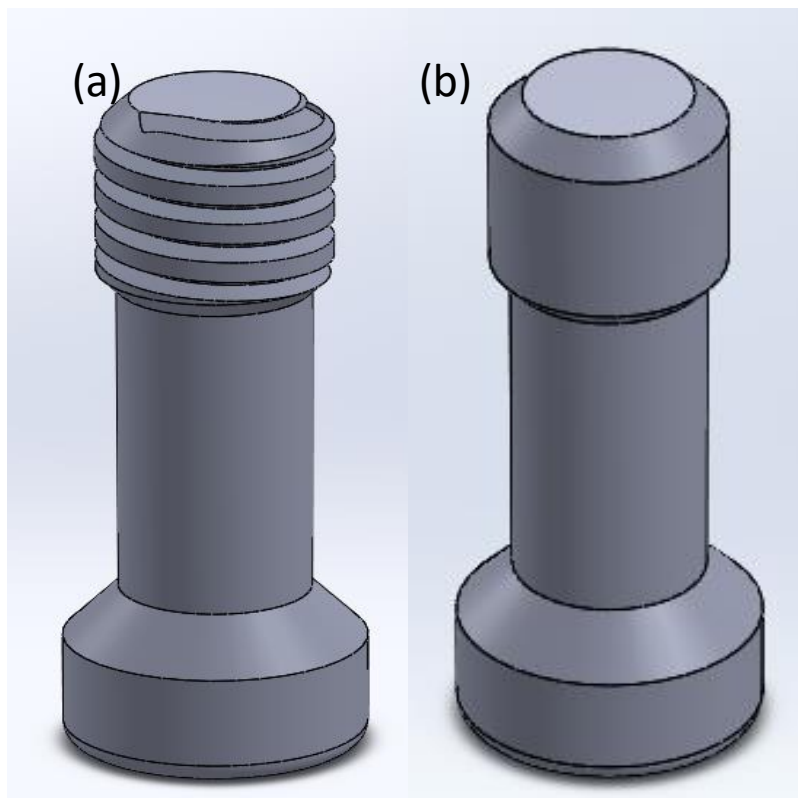

Figure A.5: Nozzle diameter of the printer.

UNIVERSITAT POLITÈCNICA DE CATALUNYA
BARCELONA**TECH**
Escola d'Enginyeria de Barcelona Est

9.1.2. Annex A2 SolidWorks

Solidworks is a computer-aided design (CAD) software for 2D and 3D modelling. This software was used to design the shape of the implant to have the plans for milling and printing, to print it was necessary to save the file as .AFM.

9.2. Annexe B: Drawings

The plans were adapted from a design submitted by Straumann. In the **Figure B.1** is shown the model of the implant with thread and the simplified, which is the one that has been finely used in this Bachelor's degree project to make the print. In the **Figure B.2** is shown the plan made from the parts modelled in 3D with SolidWorks. It should be noted that M2.20 is Straumann notation.

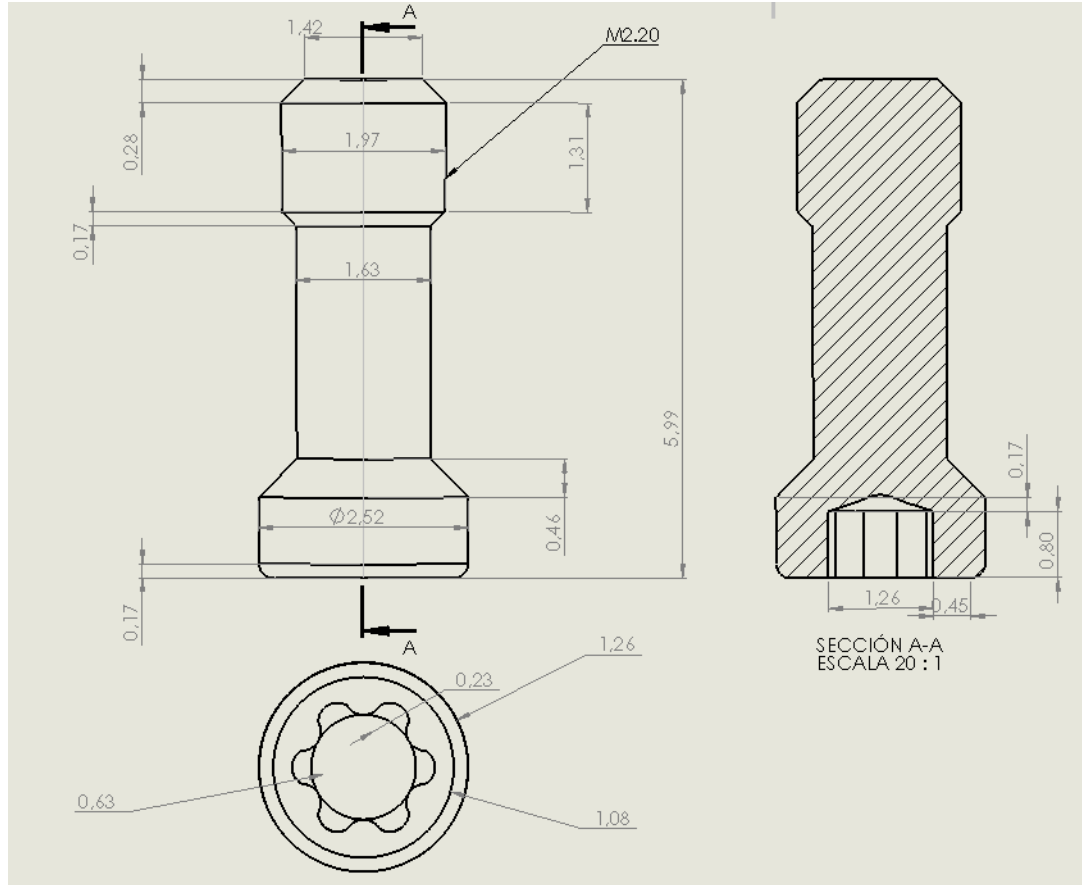**Figure B.1**: (a) model with the thread, (b) simplified model.

UNIVERSITAT POLITÈCNICA DE CATALUNYA
BARCELONATECH
Escola d'Enginyeria de Barcelona Est

Figure B.2: Drawing of the implant design. [a]